Newcastle University

ePrints

Notini L, Latta DE, Neumann A, Pearce CI, Sassi M, N'Diaye AT, Rosso KM, Scherer MM. The Role of Defects in Fe(II)-Goethite Electron Transfer. *Environmental Science & Technology* 2018, 52(5), 2751–2759.

Copyright:

This document is the Accepted Manuscript version of a Published Work that appeared in final form in *Environmental Science & Technology*, copyright © American Chemical Society after peer review and technical editing by the publisher. To access the final edited and published work see https://doi.org/10.1021/acs.est.7b05772

DOI link to article:

https://doi.org/10.1021/acs.est.7b05772

Date deposited:

17/03/2018

Embargo release date:

06 February 2019

Newcastle University ePrints - eprint.ncl.ac.uk

The Role of Defects in Fe(II)-Goethite Electron Transfer

Luiza Notini[1], Drew E. Latta[1], Anke Neumann[2], Carolyn I. Pearce[3], Michel Sassi[3], Alpha T. N'Diaye[4], Kevin M. Rosso[3], and Michelle Scherer[1,*]

[1]Department of Civil and Environmental Engineering, University of Iowa, Iowa City, IA, 52242, United States.
[2]School of Engineering, Newcastle University, Newcastle upon Tyne, NE1 7RU, United Kingdom.
[3]Pacific Northwest National Laboratory, Richland, WA 99352, United States
[4]Advanced Light Source, Lawrence Berkeley National Laboratory, Berkeley, CA 94720

*Corresponding author: Tel.: 319.335.5654; Fax: 319.335.5660; E-mail: michelle-scherer@uiowa.edu

Submitted to *ES&T*
January 26 2018

ABSTRACT

Despite substantial experimental evidence for Fe(II)-Fe(III) oxide electron transfer, computational chemistry calculations suggest that oxidation of sorbed Fe(II) by goethite is kinetically inhibited on structurally perfect surfaces. Here we used a combination of ^{57}Fe Mössbauer spectroscopy, synchrotron X-ray absorption, and magnetic circular dichroism (XAS/XMCD) spectroscopies supported by density functional theory calculations to investigate whether Fe(II)-goethite electron transfer is influenced by defects. Specifically, Fe L-edge and O K-edge XAS indicates that the outermost few Angstroms of goethite synthesized by low temperature Fe(III) hydrolysis is iron deficient relative to oxygen. Corresponding XMCD shows that this non-stoichiometric surface displays uncompensated octahedral Fe^{3+} that is weakly ferrimagnetic. This non-stoichiometric goethite undergoes facile Fe(II)-Fe(III) oxide electron transfer, depositing additional goethite consistent with experimental precedent. Hydrothermal treatment of this goethite at 150 °C, however, imparts bulk stoichiometry and antiferromagnetism at the surface. Hydrothermal treatment decreases the amount of Fe(II) oxidation, and changes the composition of the oxidation product. When hydrothermally treated goethite was ground, surface defect characteristics as well as the extent of electron transfer were largely restored. We propose that Fe vacancies comprise the defects that enable electron transfer by providing sites into which Fe(II) can strongly bind and be oxidized by the lattice, depositing Fe(III) that propagates the goethite structure. Our findings suggest that surface defects play a commanding role in Fe(II)-goethite redox interaction, as predicted by computational chemistry. Moreover, it suggests that, in the environment, the extent of this interaction, which also likely underlies Fe(II)-catalyzed recrystallization and trace element release and incorporation, will vary depending on diagenetic history, local redox conditions, as well as being subject to regeneration via seasonal fluctuations.

TABLE OF CONTENTS ART

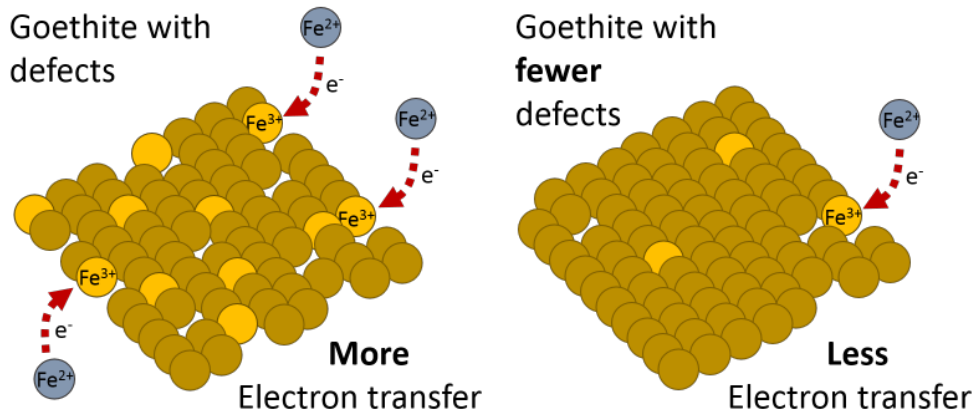

INTRODUCTION

Ferrous and ferric iron comprise one of the most abundant redox couples, and electron transfer between these two oxidation states controls the cycling and availability of Fe in water, soil, and air.[1, 2] Over the last decade significant evidence has accumulated to demonstrate interfacial electron transfer between sorbed Fe(II) and Fe(III) in Fe oxides and Fe-containing clay minerals.[3-15] In some cases, electron transfer also appears to be followed by mixing of Fe atoms from the bulk mineral structure with the surrounding fluid (also termed Fe(II)-catalyzed recrystallization).[10,16-23] While Fe(II)-Fe(III) electron transfer and mixing have been clearly demonstrated, a mechanistic understanding of these reactions remains elusive. Knowledge gaps in our understanding of Fe(II)-Fe(III) reaction mechanisms limit our ability to reliably predict important environmental and geochemical processes, such as cycling of C, N, and P,[24-29] water treatment,[30] contaminant remediation,[31-34] metal cycling,[18,35] mineral transformations,[36] and interpreting the ancient rock record.[37]

Thus far, Fe(II)-Fe(III) electron transfer has been demonstrated for several Fe oxides, including hematite, goethite, magnetite, ferrihydrite, as well as Fe-containing clay minerals.[3-15] Of the Fe minerals, electron transfer between Fe(II) and goethite has been the most extensively studied. Oxidation of Fe(II) by goethite has been shown to occur over a range of Fe(II) concentrations, amounts of Al-substitution, and in the presence of various anions, such as phosphate, bicarbonate, silicate and organic matter.[3,4,6,8,10,12,16,17]

Despite abundant experimental evidence for Fe(II)-Fe(III) oxide electron transfer, computational evidence suggests that Fe(II)-goethite electron transfer is not energetically favored on structurally perfect surfaces.[38-40] For example, density functional theory (DFT) calculations of Fe(II) adsorbed onto charge neutral, stoichiometric goethite (110) surfaces suggest that the oxidation of sorbed Fe(II) by lattice Fe(III) is energetically uphill. Others similarly conclude that charge only minimally delocalizes between Fe(II) and surface Fe(III), with only a minor dependence on the type of Fe(II)-mineral complex formed.[39,40] Additionally, a recent molecular dynamics study examining the electron transfer kinetics for stable inner and outer-sphere Fe(II) complexes on a wide range of perfect goethite terminations showed that the energetics are at best only thermoneutral, with large activation energies.[41]

Each of these studies, however, suggest or infer that surface defects may underlie the experimentally observed interfacial electron transfer.[38-40] For example, calculations simulating an oxygen vacancy on goethite (110) showed that electron transfer to the resulting lower-coordinated Fe(III) was more energetically favorable and less kinetically inhibited. This idea is conceptually similar to the notion that defects provide traps in the interior of the solid for excess electrons to accumulate.[9,42] Given these computational findings, experiments designed to test the prospective role of defects could help advance our mechanistic understanding of Fe(II)-Fe(III) oxide electron transfer.

Defects arise from a deviation in the perfect composition and/or structure of a mineral. Such features are common in goethite[43-47] and have been previously studied in terms of their relationship to growth conditions,[43,44,46,48] including non-classical growth pathways such as

imperfect oriented attachment.[49-51] The type and concentration of defects strongly influence goethite properties (e.g., *a*-dimension of the unit cell,[43] Néel temperature,[47,52,53] magnetic moment[45,53-55]) and particle reactivity (e.g., dissolution rates and ion sorption). Defects in the ideal goethite stoichiometry (i.e., α-FeOOH) can take the form of iron or oxygen vacancy, but often can be characterized as an excess of water/hydroxyl relative to the theoretical formula,[46] such that the effective formula is $\alpha\text{-}Fe_{1-y/3}O_{1-y}(OH)_{1+y}$.[43] Changes in goethite properties after hydrothermal treatment have been interpreted to be due to removal of defects.[43,44,56] Conversely, ball-milling has been suggested to add defects to goethite based on observed changes in the Néel temperature.[45]

While there is clear evidence that defects are often present in goethite, little is known about how defects influence Fe(II)-goethite electron transfer. To date, no experimental data has been presented that specifically evaluates the role of defects in Fe(II)-goethite electron transfer, despite significant speculation about their role in enabling electron transfer and driving Fe(II)-catalyzed Fe oxide recrystallization.[19, 21, 38-40] Here we provide the first experimental evidence that shows defects influence the extent of Fe(II)-goethite electron transfer and the composition of the product formed**.** Our findings indicate that low temperature Fe(III) hydrolysis results in goethite particles that have excess hydroxyl/water content and corresponding Fe vacancies that enable Fe(II)-goethite electron transfer. Hydrothermally treating the goethite particles appears to remove defects, inhibit Fe(II)-goethite electron transfer, and alter the composition of the oxidation product. Our findings suggest that surface defects play an important role in Fe(II)-goethite redox interaction, as predicted by computational chemistry.

METHODS

Oxide Synthesis. Goethite was prepared from ^{56}Fe-enriched Fe metal ((Isoflex, 99.94% purity), ^{56}Fe goethite) by modifying the Schwertmann and Cornell method, using iron metal as the synthesis' starting point instead of $Fe(NO_3)_3$.[57] Briefly, ^{56}Fe(0) was dissolved in HCl to obtain 15 mL of an Fe(II) stock (~ 0.6 M Fe(II), ~ 1.8 M HCl), and the solution was oxidized using 2 mL of 30% (slight excess) H_2O_2 to produce Fe(III). Then, the pH was raised with 16 mL of 5 M KOH and the resulting precipitate was placed in an oven at 70 °C for 60 hours. ^{56}Fe goethite was washed, centrifuged, freeze dried, ground with a mortar and pestle, and passed though a 100 mesh sieve. The final mineral is referred to as "as-synthesized" and it is similar to the microgoethite used in our previous work.[3,6,10,12,16,17] The Brunauer-Emmett-Teller (BET) specific surface area was determined by N_2 soprtion at 77 K and found to be 28 to 34 $m^2\ g^{-1}$. X-ray diffraction (XRD - Rigaku Mini FlexII) patterns showed that the material contains goethite and no other minerals (**Figure S7**).

Electron Transfer Experiments. All experiments were carried out in an anaerobic glovebox with N_2/H_2 atmosphere (93/7%), and all solutions were purged at least 2 hours with N_2 prior to trasfer into the glovebox. Fe(II) stock solutions were prepared inside the glovebox by reacting ^{57}Fe metal (Cambridge Isotope, 96.93% purity) with 1 M HCl overnight. The resulting solution was filtered to remove any residual Fe(0) and diluted with deionized (DI) water to the desired concentration (~ 100 mM Fe(II), ~ 0.1 M HCl).

Batch reactors were prepared by adding 10 mL of 25 mM HEPES (4-(2-hydroxyethyl)-1-piperazineethanesulfonic acid), pK_a 7.55[58]) buffer adjusted to pH 7.5 ± 0.05 plus 25 mM KBr electrolyte to a 20 mL glass vial and adding Fe(II) stock to reach an initial ^{57}Fe(II) concentration of ~1 mM. The reaction was started by adding 20.0 ± 0.2 mg of ^{56}Fe goethite and the reactors were placed on a end-over-end rotator in the absence of light. The aqueous phase was filtered (0.2 μm) and acidified with trace metal grade HCl for subsequent Fe(II) and total Fe analysis using the 1,10-phenanthroline method.[59]

Extraction. Two additional reactors were prepared by reacting ^{56}Fe goethite with ^{57}Fe(II), and the reacted solids were centrifuged and then extracted to remove the sorbed Fe species. The first reactor was extracted with a 0.4 M HCl (15 minutes). For the second reactor, the reacted solids were subjected to a sequential extraction procedure using HEPES buffer (pH 7.5, 1 hour) followed by 1 M $CaCl_2$ (pH 7, 4 hours) and 1 M NaH_2PO_4 (pH 5, 18 hours). A 30 min wash step with DI water was carried out after the $CaCl_2$ and NaH_2PO_4. The extracted solids were analyzed by Mössbauer spectroscopy and the extracted aqueous phase were analyzed for Fe(II) and total Fe.

Hydrothermal treatment. Goethite was subjected to a hydrothermal treatment to anneal defects. A suspension of the as-synthesized ^{56}Fe goethite in deionized water was placed into a digestion bomb, and kept in an oven at 150 °C for 44 hours. The digestion bomb was allowed to cool down and the solids were centrifuged and freeze dried (refered to as hydrotermally treated goethite). The batch of hydrothermally treated goethite was split in two, and part of it was reacted with 1 mM ^{57}Fe(II) as discussed above. The other part was crushed with mortar and pestle to restore defects (referred to as ground goethite). Again, the batch was split, and part was reacted with 1 mM ^{57}Fe(II), while the other aliquot was hydrothermally treated again under the same conditions, and then reacted with 1 mM ^{57}Fe(II) (refered as hydrothermally treated *again* goethite).

Samples of goethite after sequetial treatments were characterized by XRD, scanning electron microscopy (SEM - Hitachi S-4800), transmission electron microscopy (TEM - JEOL JEM 1230), X-ray absorption spectroscopy (XAS) and X-ray magnetic circular dichroism spectroscopy (XMCD).

Mössbauer spectroscopy. For Mössbauer spectroscopy, solids were collected on a 0.2 μm nitrocelulose filter and than sealed between two pieces of Kapton tape to avoid air oxidation. Mössbauer spectra were collected at 77 K on a spectrometer supplied by Web Research, Inc. (Edina, Minnesota, USA) and equipped with closed-cycle cryostat (CCS-850 System, Janis Research Co., Wilmington, Massachusetts, USA). We acquired spectra in transmission mode using a constant acceleration drive system and a ^{57}Co source. The velocity scale was calibrated using a 7-μm α-Fe(0) foil. We fit the spectra using the software Recoil (Ottawa, Canada).[60]

Selected samples were reanalyzed after atmosphere exposure. After initial Mössbauer analysis, these samples were stored for a month in normal atmosphere and then reanalyzed by Mössbauer spectroscopy. For comparison, one sample was kept inside the anaerobic glovebox for the same time span.

Synchrotron X-Ray Absorption and Magnetic Circular Dichroism Spectroscopy. For X-ray absorption spectroscopy, suspensions of goethite were dropped onto indium foil in an anaerobic glovebox with N_2/H_2 atmosphere (93/7%), dried, then pressed into the foil and the excess solid was removed. The indium foil was attached to the copper sample manipulator with silver paint. XAS and XMCD measurements were performed using Beamline 6.3.1.1 at the Advanced Light Source (Berkeley, CA). Fe $L_{2,3}$-edge and O K-edge XAS were recorded at room temperature in total electron yield mode; Fe $L_{2,3}$-edge XAS has an effective probing depth of 50 Å. Fe $L_{2,3}$-edge XMCD spectra were obtained by measuring two XAS spectra with a fixed degree of circular polarization of ~ 0.7 and with opposing magnetization directions by reversing the applied field of 1.8 T at each energy point. The XAS spectra were normalized to incident beam intensity, and the XMCD spectrum was obtained as the difference between the two spectra.

Density Functional Theory Computations. We used the FDMNES code[61] to individually calculate the O K-edge XANES spectra of the two oxygen sites present in goethite, explicitly taking into account their respective local coordination environments in the bulk structure. The Green's formalism approach, within the limit of the muffin-tin approximation, was used. The Fermi energy has been determined self-consistently using an aggregate of radii of 7 Å. A cluster of 7 Å radii has also been used to perform the final state calculations. The Hedin-Lundquist potentials[62] were used to model the exchange-correlation. Dipoles, core-hole contributions and spin-orbit coupling were taken into account. Because the experimental spectra of goethite is made of two components with unknown relative position and intensity, we have used a non-negative least square algorithm to refine the position and intensity of the two calculated O^{2-} and OH^- component spectra, and have found the best linear combination that would fit the experimental spectra. The resulting linear combination fit of the measured O K-edge spectra with the computed component spectra for O^{2-} and OH^- was used to quantify relative contributions of these two oxygen species.

RESULTS AND DISCUSSION

Fe(II)-Goethite Electron Transfer. To explore if defects influence Fe(II)-goethite electron transfer, we ran a series of Fe isotope labeled experiments with as-synthesized and hydrothermally treated goethite particles. Similar to our previous work[3,5,6,10-12,14], we took advantage of the element and isotope specificity of ^{57}Fe Mössbauer spectroscopy to track if Fe(II)-goethite electron transfer occurs. Here, we treated Mössbauer-invisible ^{56}Fe goethite with a sequence of hydrothermal treatment and grinding steps in an attempt to remove or add defects, presumably at surfaces, and then reacted the goethite with 1 mM ^{57}Fe(II) and collected ^{57}Fe Mössbauer spectra of the filtered solids to determine if sorbed Fe(II) was oxidized (**Figure 1**). The ^{57}Fe Mössbauer spectra of the reacted solids revealed two prominent Fe(III) sextets consistent with goethite and suggest that substantial oxidation of ^{57}Fe(II) occurred and formed ^{57}goethite on both the as-synthesized goethite and the hydrothermally treated goethite (**Table S1**). Oxidation of sorbed Fe(II) by goethite is consistent with our and others' previous work.[3,6,8,10,12]

After reaction with ^{57}Fe(II), there is, however, a marked difference between the as-synthesized goethite and the hydrothermally treated goethite. The Fe(III) sextets capture a smaller portion of the spectral area of the hydrothermally treated compared to the as-synthesized goethite (as shown by blue sextets in **Figure 1a and b)**. To test if the change in spectral area distribution upon hydrothermal treatment was reversible, we ground the hydrothermally treated goethite particles and reacted them with ^{57}Fe(II). The resulting spectrum shows a marked increase in the amount of area captured by the sextet (and less hatched area) (**Figure 1c**). A second hydrothermal treatment returned the spectrum of Fe(II)-reacted solids to one similar to that of the first hydrothermal treatment (**Figure 1d**). To test that the change in spectral area trend observed in **Figure 1** was not particular to a goethite synthesis batch, we ran duplicates of each treatment using two separate batches of goethite (**Figure S1**). The similarity of the duplicate experiments conducted with two separately synthesized goethite batches provides strong evidence that hydrothermal treatment and grinding are reproducibly altering the goethite in a way that influences how it reacts with Fe(II).

The reversible, reproducible changes in the Mössbauer spectra indicate that hydrothermal treatment and grinding are influencing the product formed from ^{57}Fe(II) interaction with goethite. To fit the hatched area in the Mössbauer spectra we tried a variety of approaches**.** We concluded that the best method to capture the hatched area was to include an Fe(II) doublet and a broad, collapsed sextet consistent with our and other's previous approach (for more details see SI and **Figure S2)**.[10,63] Small Fe(II) doublets comprising less than 10% of the total area have been previously observed in spectra of goethite reacted with ^{57}Fe(II),[8,10,12] but little is known about the composition of the broad, collapsed sextet and we have, in our previous work, been careful to not interpret it beyond that it was likely Fe(III).[10] To check whether that the collapsed feature was influenced by buffer-Fe interactions[64], we ran a control experiment without buffer (**Figure S4**). There was no difference between the spectra of the buffered and un-buffered samples indicating that the buffer-Fe interactions were not responsible for the collapsed feature.

To investigate the composition of the collapsed feature, we subjected the as-synthesized goethite particles reacted with ^{57}Fe(II) to different extraction procedures and collected Mössbauer spectra afterwards (**Figure 2**). A mild HCl extraction (0.4 M) removed both the Fe(II) doublet and the broad, collapsed sextet from the Mössbauer spectra. All of the Fe(II) that had initially sorbed was recovered in the HCl extract (**Table S2**). Surprisingly, the aqueous extract from the HCl treatment contained only Fe(II), suggesting that the collapsed feature was at least partially due to Fe(II). To minimize the change in pH during extraction, we also extracted goethite reacted with ^{57}Fe(II) with $CaCl_2$ and NaH_2PO_4 which only decreased the pH to 7 and 5, respectively. Similar to the HCl extraction, the milder extractions removed most of the collapsed feature and recovered similar amounts of Fe(II) (for additional discussion see SI and **Figure S5).**

As an alternative approach to evaluate whether the collapsed feature contains Fe(II), we oxidized a sample of goethite reacted with ^{57}Fe(II) to see if the collapsed feature disappeared. One month of air exposure resulted in complete removal of the collapsed feature and the Fe(II) doublet from the spectra, providing an additional line of evidence that the collapsed feature

contained some Fe(II) (**Figure 2**). The spectra of the oxidized goethite, however, looks slightly different than the spectra of the HCl-extracted goethite, in which a third sextet appeared. The third sextet was identified as akaganéite, a mineral typically formed by the hydrolysis of Fe(III) salts in the presence of Cl^-.[65] Regardless of the precise identity of the collapsed feature, the oxidation and extraction data combined provide compelling evidence that the collapsed feature contains some Fe(II) and is more likely a mixed Fe(II)-Fe(III) phase rather than a pure Fe(III) phase as we previously thought.[10] While we cannot rule out that it is a pure Fe(II) phase, the Mössbauer parameters of the collapsed sextet are more consistent with a mixed Fe(II)-Fe(III) compound (further discussed in **Supporting Information**).[66] Importantly, the presence of a mixed Fe(II)-Fe(III) phase rather than an Fe(III) phase suggests that some of ^{57}Fe(II) sorbed on goethite was not oxidized by the goethite.

To quantify the extent of sorbed Fe(II) that was oxidized to goethite as a function of surface treatment, we plotted the percent relative area of the two goethite sextets for the as-synthesized goethite and the successive hydrothermally treated and ground goethite particles (**Figure 3**). If one hundred percent of the spectral area was captured within the two goethite sextets, it would indicate that all of the sorbed ^{57}Fe(II) was oxidized to ^{57}goethite. Complete oxidation of Fe(II) did not occur in any of the samples, but instead the amount of Fe(II) oxidized to form goethite varied between 63 and 87% (as estimated from the relative area of the sextets). What is most striking in **Figure 3**, however, is how reversible and reproducible the hydrothermal and grinding treatment is in influencing the extent of oxidation of the goethite-sorbed Fe(II). The as-synthesized goethite oxidized ≈ 87% of the sorbed Fe(II) to form goethite, whereas hydrothermally treating the goethite particles resulted in only ≈ 66% of the sorbed ^{57}Fe(II) becoming oxidized to goethite, suggesting that electron transfer was inhibited by hydrothermal treatment and that the composition of the oxidation product changed. Grinding the hydrothermally treated goethite largely restored the extent of electron transfer (≈ 81%), and hydrothermally treating this goethite sample *again* inhibited the extent of electron transfer (≈ 63%) (**Figure 3)**.

Similar to the as-synthesized goethite, one month of air exposure of the hydrothermally treated goethites resulted in removal of the collapsed feature and the Fe(II) doublets from the spectra, consistent with the collapsed feature containing some Fe(II) (**Figure S6**). The hydrothermally treated goethites reacted with ^{57}Fe(II) also lost substantially more spectral area than the ground samples (as-synthesized and ground goethite), providing additional evidence that hydrothermally treating goethite leads to less oxidation of sorbed Fe(II) to goethite.

Bulk Characterization of Goethite Particles. It appears that hydrothermal treatment and grinding reversibly and reproducibly influences the extent of electron transfer from sorbed Fe(II) to goethite as well as the composition of the oxidation product. Given previous evidence that goethite synthesis conditions such as temperature alter the defect content in goethite,[43,44] we hypothesized that hydrothermally treating the goethite particles at 150 °C annealed defects present in the goethite synthesized at 70 °C. We further hypothesized that grinding the particles added defects back to the hydrothermally treated particles. To evaluate if there were any changes

in the bulk goethite particles before and after treatments, we characterized the particles with XRD, BET analysis, and microscopy. XRD spectra of treated solids confirmed that hydrothermal treatment did not transform goethite into any other mineral (**Figure S7**), and cell dimensions were unchanged after the goethite sequential hydrothermal/grinding treatments (**Table S3**). Schwertmann and collaborators observed a slight change in the *a*-axis dimension upon hydrothermal treatment, however, their initial material was a highly defective goethite.[43] BET measurements revealed a small, but progressive loss in BET area (from 28 to 19 $m^2\ g^{-1}$, **Table S3**), consistent with previous observations.[43,44,56] In our work, TEM images revealed no substantial difference between as-synthesized and hydrothermally treated goethite, but SEM images revealed slight changes of the surface (**Figure S8 and S9**). Hydrothermally treated goethite appeared to have more perfectly formed ends when compared to the original mineral suggesting the hydrothermal treatment may have removed some surface defects (**Figure S9**).

Because hydrothermal treatment resulted in smaller BET surface area and amounts of Fe(II) sorbed, we considered the alternative hypothesis that less Fe(II)-goethite electron transfer could be simply due to less surface area and less surface-bound Fe(II) available to be oxidized. To explore whether the amount of sorbed Fe(II) influenced the extent of electron transfer, we plotted the percent relative area of the Fe(III) sextets versus sorbed Fe(II) per m^2 (**Figure 4**). We binned the data into ground goethites which includes as-synthesized and ground (colored markers) and hydrothermally treated goethites which includes both rounds of hydrothermal treatment (open markers). Both ground and hydrothermally treated goethites converge to ~5.5 μmoles Fe(II) sorbed per m^2, revealing that the sorption of Fe(II) was not influenced by the treatment applied to the mineral. However, it is remarkable that, when we compare a hydrothermally treated and a ground goethite that have the same amount of Fe(II) sorbed per m^2, there is a marked difference ($\approx 20\%$) in the extent of electron transfer. **Figure 4** provides compelling evidence that the changes we observed in Fe(II)-goethite electron transfer between our four treatments were not due to changes in surface area or amount of Fe(II) sorbed.

Surface Characterization of Defects on Goethite Particles. While bulk characterization of the treated goethite particles is informative, it is unlikely we would be able to detect specific changes in goethite surface structure with these techniques. To detect the presence of defects and changes in surface structure in the treated goethites, we collected X-ray absorption spectroscopy (XAS) and X-ray magnetic circular dichroism (XMCD) at the Fe L-edge and XAS at the O K-edge. By collecting total electron yield data, these techniques probe a depth no greater than 5 nm and are mainly sensitive to the upper few Angstroms.[67] Fe L-edge XMCD spectra for all three samples is shown in **Figure 5**, while the illustrative O K-edge spectra and DFT-based spectral analysis are shown in **Figure 6**.

The Fe L-edge XAS probes the structure and valence of surface iron, whereas the XMCD is selective for the subset of surface iron that is magnetically ordered and is able to discriminate Fe valence and local coordination. As expected, the Fe L-edge XAS of all goethite samples measured shows features consistent with goethite Fe(III); Fe(II) is not detected (**Figure S10**). The corresponding XMCD information, however, is more revealing (**Figure 5**). The as-

synthesized goethite has a weak magnetic moment at the surface (i.e., from the magnetic dichroism signal intensity), and the shape of the XMCD signal is consistent with octahedrally coordinated Fe(III).[68] The presence of this magnetic moment indicates that the surface is magnetic, likely due to Fe vacancies that disrupt the antiferromagnetic symmetry that would otherwise exist between perfect atomic planes of goethite.[52] The XMCD signal of the hydrothermally treated goethite contains no distinguishable feature, indicating that the magnetic moment is absent, which is consistent with the known bulk antiferromagnetic structure and the hypothesis that hydrothermal treatment yields a more stoichiometric and crystalline material. After re-grinding, the surface magnetic moment, and thus XMCD trace, is largely restored, consistent with reintroduction of Fe vacancies at the surface.

The corresponding O K-edge XAS spectra are illustrated in **Figure 6**, and analyzed in more detail in the SI and **Figures S11** and **S12**. The spectral region of primary interest is the pre-edge region between 530-535 eV, which is comprised of two $1s \rightarrow 3d$ excitation doublets, one at lower energy corresponding to O^{2-} in the goethite surface, and one at higher energy corresponding to OH^- in the surface.[69] Using DFT, we computed the specific expected shapes of these two doublets and used these theoretical components to perform linear combination fitting (LCF) of the experimentally measured O K-edge spectra for the three goethite samples. We then determined the OH/O^{2-} ratio for the surfaces of each of three goethites. Additionally, the ratio of the measured total integrated Fe L-edge and O K-edge XAS intensities were used to estimate the Fe/O ratios in each of the three surfaces. Here we used the hydrothermally treated goethite as a normalization standard to the bulk ratio of 0.5 under the assumption that this surface is the most stoichiometric within the set. The complete surface compositional results are given in **Table 1**.

The O K-edge spectra for as-synthesized, hydrothermally treated and ground goethites show that the surfaces of the as-synthesized and ground goethite are more hydrous (OH^- rich relative to O^{2-}) than the hydrothermally treated goethite (**Figure 6** and **Table 1**). Note that while the bulk ideal OH/O^{2-} ratio is 50%, the excitation cross-sections of the two component spectra are not necessarily equivalent such that a ratio of their integrated intensities could be expected to also correspondingly be 50%; we chose not to normalize these ratios to the ideal value because the trends between samples remain the same in either case. Surfaces of as-synthesized and ground goethite bear comparably lower Fe/O ratios relative to the hydrothermally treated goethite (**Table 1**), again consistent with the prevalence of Fe vacancies in these two surfaces relative to the hydrothermally treated surface.

Collectively, the observed surface compositional characteristics are consistent with the known behavior of goethite stoichiometry to vary as α-$Fe_{1-y/3}O_{1-y}(OH)_{1+y}$. Due to excess protons, goethite grown at sub-hydrothermal temperatures, e.g. 70 °C as used here, tends to be both Fe deficient and correspondingly OH-rich. In contrast, goethite grown hydrothermally tends to be more crystalline and stoichiometric.[43] Combined, the results from Mössbauer spectroscopy, XAS, and XMCD suggest that particles with fewer defects are less prone to oxidize Fe(II). We propose that the key surface defects are Fe vacancies, which provide sites into which Fe(II) can strongly bind and transfer electrons to lattice Fe(III), propagating a goethite-like surface. Our findings

suggest that surface defects play a commanding role in Fe(II)-goethite redox reaction, as predicted by computational chemical modeling.[38-40]

Environmental Implications

Here we provide the first experimental evidence that defects influence the extent of Fe(II)-goethite electron transfer and the composition of the product formed. Our findings indicate that low temperature Fe(III) hydrolysis, a commonly used method for synthesizing goethite, results in goethite particles that have excess hydroxyl/water content and corresponding Fe vacancies that enable Fe(II)-goethite electron transfer. Hydrothermally treating the goethite particles appears to remove defects, inhibit Fe(II)-goethite electron transfer, and alter the composition of the oxidation product. The clear role of defects in enabling Fe(II)-goethite electron transfer resolves the previous discrepancy between multiple experimental observations of Fe(II)-goethite electron transfer[3, 4, 6, 8, 10, 12, 16, 17] and computational calculations that suggest Fe(II)-goethite electron transfer is not energetically feasible on structurally perfect surfaces.[38-40]

Our experimental evidence that defects enable Fe(II)-goethite electron transfer raises the question of whether defects influence Fe(II)-catalyzed recrystallization as we and others have proposed that Fe(II)-Fe(III) interfacial electron transfer is an integral step in Fe(II)-catalyzed recrystallization,[7, 9, 16, 70, 71] While there has been speculation that mineral surface and structural defects control Fe(II)-catalyzed recrystallization[19, 21] experimental data to evaluate this claim is lacking. If Fe(II)-Fe(III) oxide electron transfer controls the extent of Fe oxide recrystallization than our results support the hypothesis that defects play a role in Fe(II)-catalyzed recrystallization. We further speculate that the removal of defects to form a more perfect surface may be the energetic driving force for Fe(II)-catalyzed recrystallization that has continued to elude us. We caution, however, that alternative mechanisms of recrystallization such as solid-state diffusion or pore/void/intergranular diffusion[16, 19] have not been ruled out and neither of these mechanisms are likely to be as strongly influenced by electron transfer.

The role of defects in Fe redox chemistry also provides valuable insights into the behavior of Fe oxides in reducing environments. If defects in the form of Fe deficient and OH-rich surfaces enable Fe(II)-goethite electron transfer, then it seems reasonable to suggest that oxidative sorption of Fe(II) at the surface would fill Fe vacancies and anneal some surface defects. Consistent with our suggestion that oxidative sorption of Fe(II) anneals surface defects, we have previously observed less oxidation of sorbed Fe(II) by hematite at high concentrations of Fe(II)[5] as well as reduced extents of hematite recrystallization.[72] Annealing of goethite by oxidative sorption of Fe(II) followed by inhibition of electron transfer may also explain the recent report of decreased goethite recrystallization rates over time.[20] Our hypothesis that oxidative sorption of Fe(II) anneals surface defects is in agreement with results that show addition of Fe(II) inhibits rates of microbial Fe(III) reduction.[73, 74] How defects will impact heterogeneous redox process such as contaminant reduction rates,[3, 33, 34, 75-78] and the observed paradoxical oxidation of As(III) at the Fe(II)-Fe oxide interface, however, remains open to experimental investigation.[8, 79, 80]

Our work also shows that electron transfer between Fe(II) and goethite is sensitive to diagenetic temperature and can be altered by relatively small changes in the structure. We note that we were only able to observe these changes with surface-sensitive techniques (i.e., XMCD and oxygen XAS). Environmental cycles that include temperature fluctuations, changes in the activity of water, and redox changes can likely reinitialize electron transfer between Fe(II) and goethite, and possibly restart recrystallization by controlling the defect content at the goethite/water interface. The small, subtle changes needed to influence Fe(II) – goethite interaction suggest that in the environment, the extent of this interaction, which also likely underlies Fe(II)-catalyzed recrystallization trace element release and incorporation,[18, 35, 70] will be coupled to diagenetic history, local redox conditions, and be subject to regeneration via seasonal fluctuations.[34, 37]

ASSOCIATED CONTENT

Supporting Information. Details on Mössbauer fitting, discussion on HCl-extracted and oxidized samples as well as additional figures of fitted Mössbauer spectra, Mössbauer spectra of duplicates and extracted samples, SEM and TEM pictures and XRD spectra of the as-synthesized and treated sample. This material is available free of charge via the Internet at

AUTHOR INFORMATION

Corresponding Author
*E-mail: michelle-scherer@uiowa.edu

ACKNOWLEDGEMENTS

This material is based upon work supported by the U.S. Department of Energy's (DOE) Office of Science, Office of Basic Energy Sciences (BES), Chemical Sciences, Geosciences, and Biosciences Division through its Geosciences program at Pacific Northwest National Laboratory (PNNL). A portion of this research was performed using EMSL, a national scientific user facility sponsored by the DOE Office of Biological and Environmental Research and located at PNNL. The work performed at the Advanced Light Source (ALS) was supported by the Director, Office of Science, BES of the DOE under Contract No. DE-AC02-05CH11231. PNNL is a multiprogram national laboratory operated for DOE by Battelle Memorial Institute under Contract No. DE-AC06-76RLO-1830. Additional support for this work was provided by the National Science Foundation (NSF) through the NSF Division of Chemistry under Grant No. 1347848.

Table 1. Summary of surface compositional analyses of goethite from X-ray absorption spectroscopy at the Fe L-edge and O K-edge, with the latter further quantified in terms of O^{2-} and OH^-, using linear combination fitting of the experimental spectra with DFT-based O K-edge doublets.

	As-synthesized	Hydrothermally Treated	Ground
Fe/O	**0.23**	**0.50***	**0.22**
OH^-	47.45%	41.73%	44.36%
O^{2-}	52.55%	58.27%	55.64%
OH^-/O^{2-}	**0.90**	**0.72**	**0.80**

(*)To normalize Fe/O ratios based on integrated intensities of separately collected Fe L-edge and O K-edge spectra, all values were scaled proportionally by the factor needed to achieve the idealized 0.50 value for the hydrothermally treated goethite.

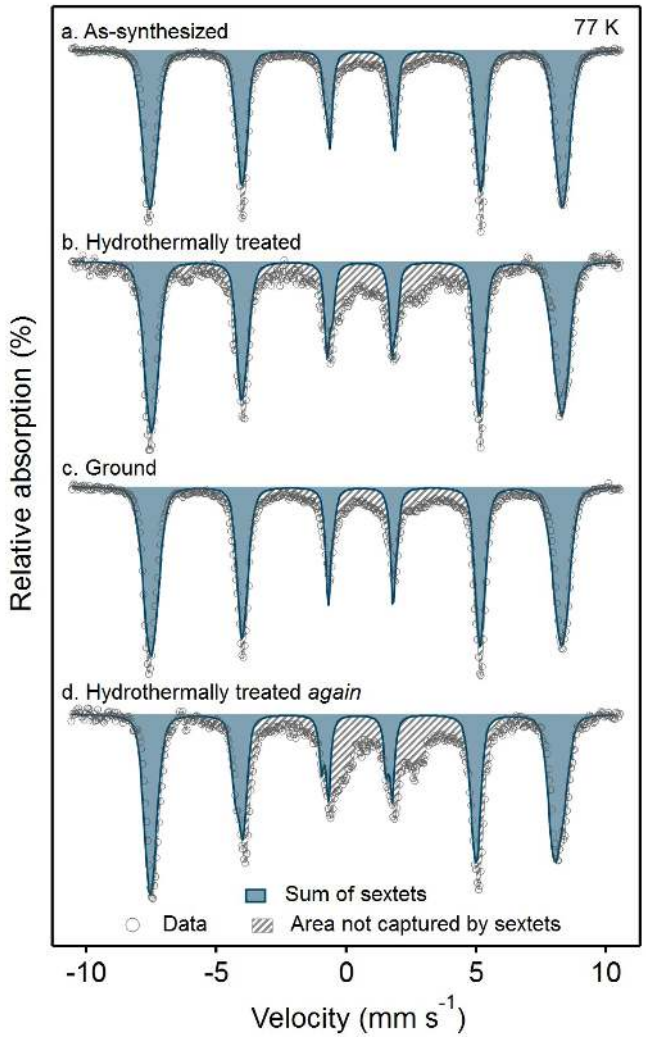

456
457
458
459 **Figure 1.** Mössbauer spectra of ^{57}Fe(II) reacted with ^{56}Fe goethite after sequential
460 hydrothermal/grinding treatments. Experimental conditions: [^{56}Gt]= 2 g L^{-1}, 25 mM HEPES/25
461 mM KBr at pH 7.5.
462

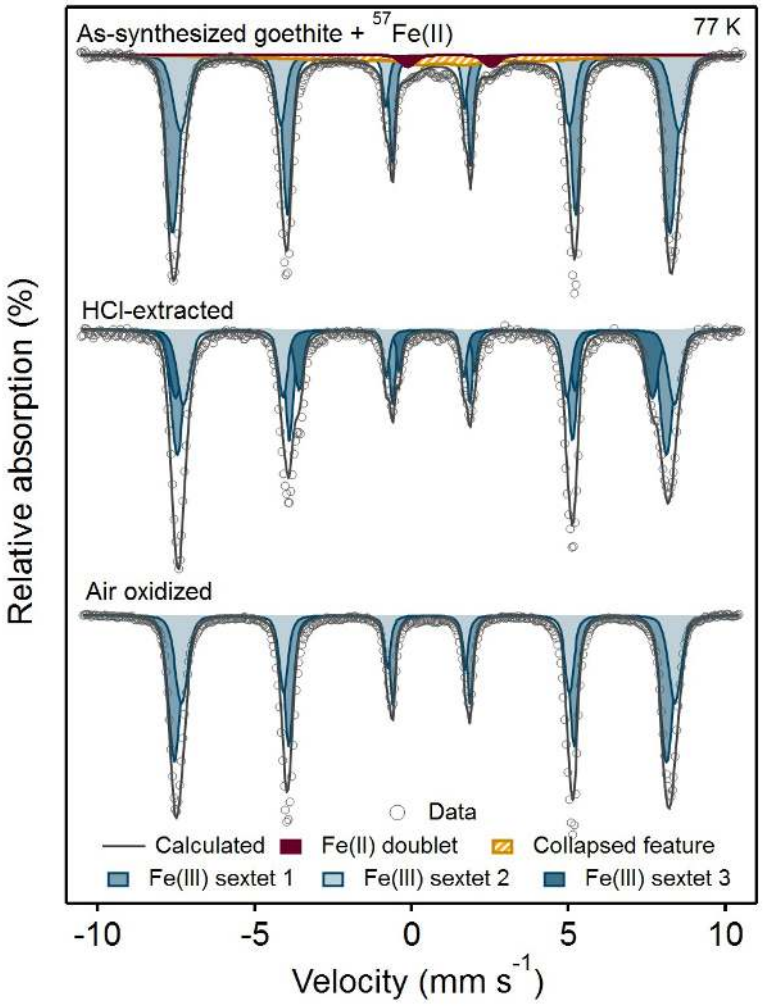

Figure 2. Mössbauer spectra of ^{56}Fe as-synthesized goethite reacted with 1 mM ^{57}Fe(II), before and after HCl extraction and air oxidation. Experimental conditions: [^{56}Gt]= 2 g L^{-1}, 25 mM HEPES/25 mM KBr at pH 7.5.

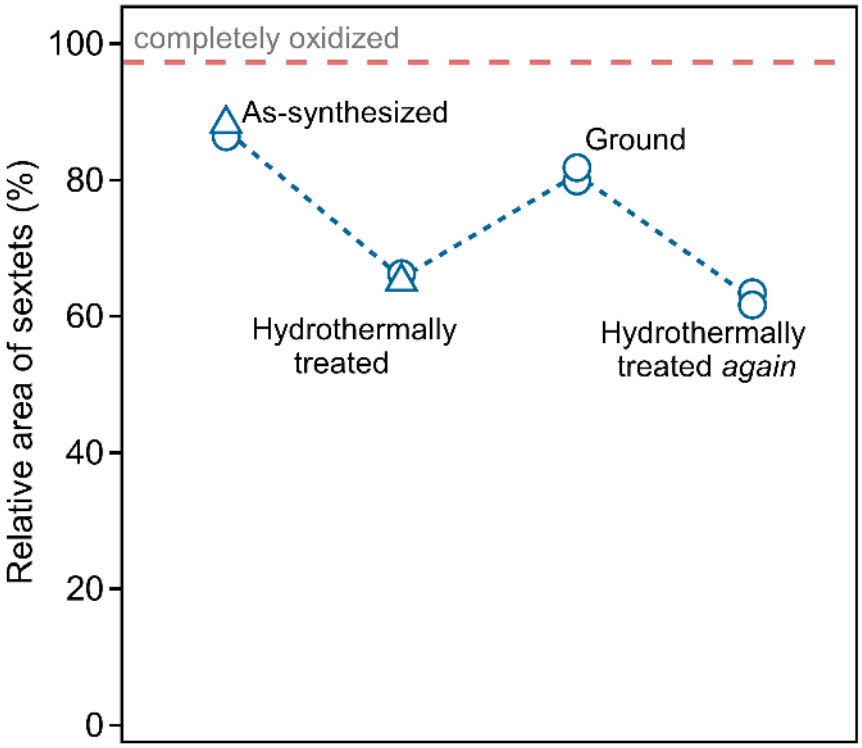

Figure 3. Relative area of Fe(III) sextets from Mössbauer spectra of ^{57}Fe(II) reacted with ^{56}Fe goethite after sequential hydrothermal/grinding treatments. Percentages based on spectral fits shown in Figure S2 (data in Table S1) and described in the SI. Different markers indicate different ^{56}Fe goethite batches. Duplicates from the same batch were hydrothermally treated/ground in separate experiments.

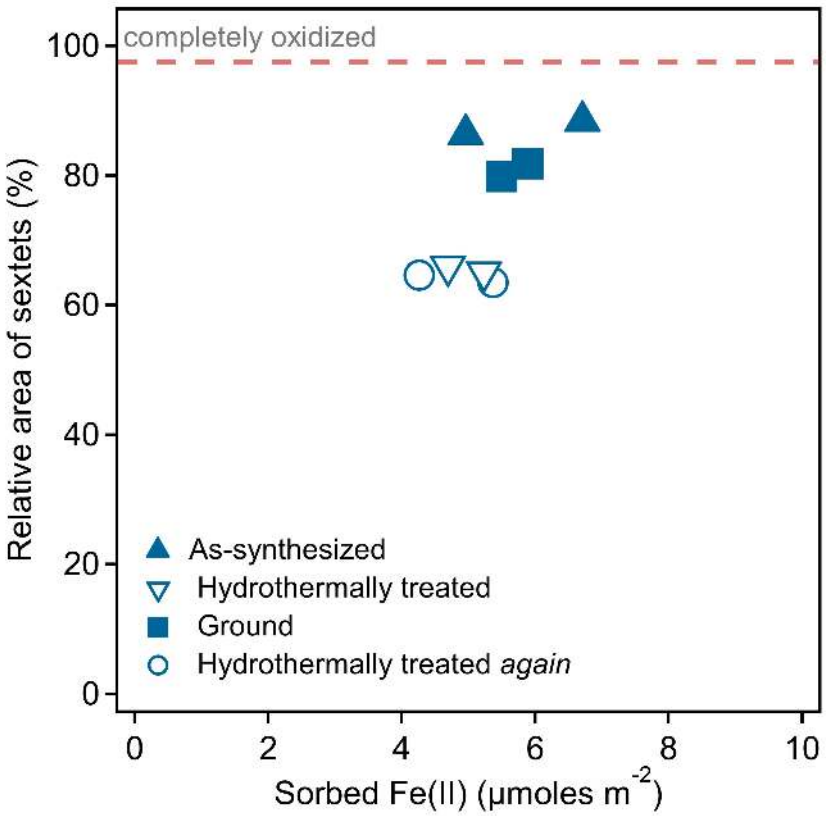

Figure 4. Relative area of Fe(III) sextets from Mössbauer spectra as a function of sorbed Fe(II) per m^2 for samples of ^{57}Fe(II) reacted with goethite after sequential hydrothermal/grinding treatments.

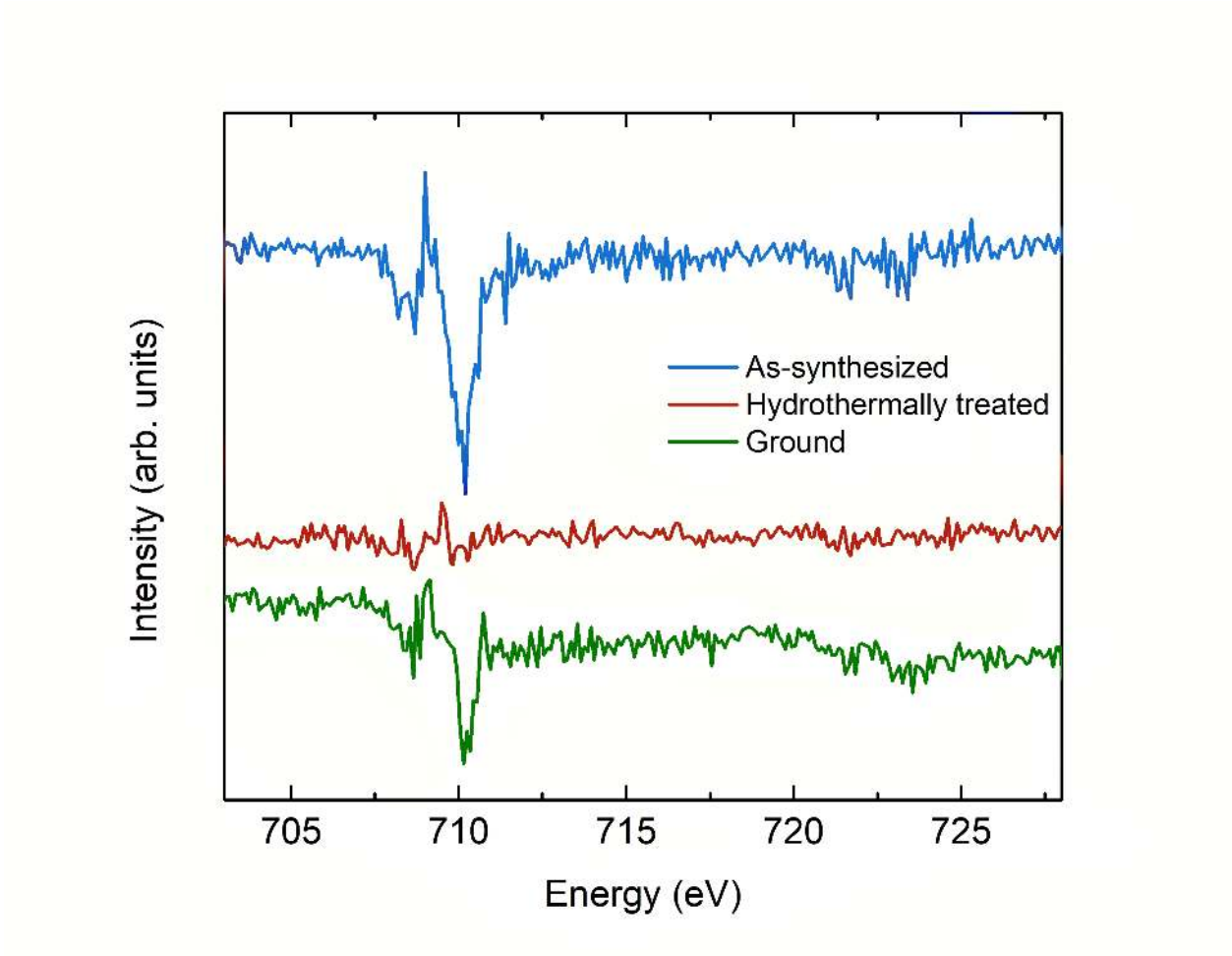

Figure 5. Fe L-edge XMCD of goethite after sequential hydrothermal/grinding treatments.

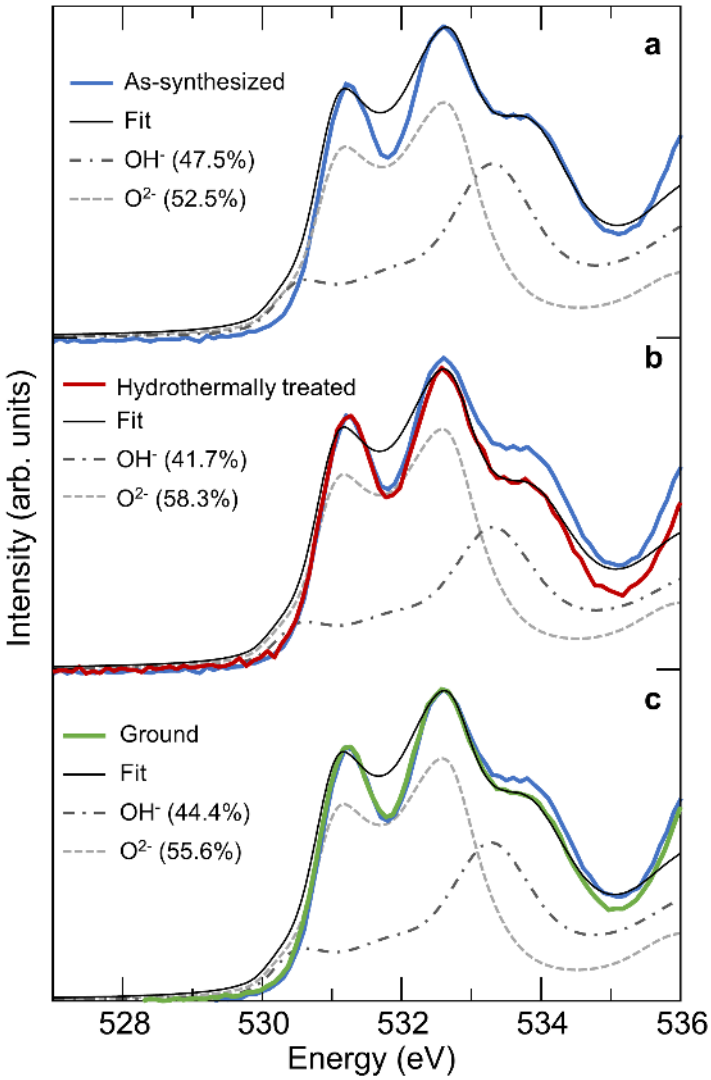

Figure 6. O K-edge XAS of goethite after sequential hydrothermal/grinding treatments.

REFERENCES

1. Stumm, W.; Sulzberger, B., The cycling of iron in natural environments: Considerations based on laboratory studies of heterogeneous redox processes. *Geochimica et Cosmochimica Acta* **1992,** *56*, (8), 3233-3257.
2. Jickells, T., Atmospheric inputs of metals and nutrients to the oceans: their magnitude and effects. *Marine Chemistry* **1995,** *48*, 199-214.
3. Williams, A. G. B.; Scherer, M. M., Spectroscopic Evidence for Fe(II)−Fe(III) Electron Transfer at the Iron Oxide−Water Interface. *Environmental Science & Technology* **2004,** *38*, (18), 4782-4790.
4. Silvester, E.; Charlet, L.; Tournassat, C.; Géhin, A.; Grenèche, J.-M.; Liger, E., Redox potential measurements and Mössbauer spectrometry of Fe^{II} adsorbed onto Fe^{III} (oxyhydr)oxides. *Geochimica et Cosmochimica Acta* **2005,** *69*, (20), 4801-4815.
5. Larese-Casanova, P.; Scherer, M. M., Fe(II) Sorption on Hematite: New Insights Based on Spectroscopic Measurements. *Environmental Science & Technology* **2007,** *41*, (2), 471-477.
6. Cwiertny, D. M.; Handler, R. M.; Schaefer, M. V.; Grassian, V. H.; Scherer, M. M., Interpreting nanoscale size-effects in aggregated Fe-oxide suspensions: Reaction of Fe(II) with Goethite. *Geochimica et Cosmochimica Acta* **2008,** *72*, (5), 1365-1380.
7. Yanina, S. V.; Rosso, K. M., Linked Reactivity at Mineral-Water Interfaces Through Bulk Crystal Conduction. *Science* **2008,** *320*, (5873), 218-222.
8. Amstaetter, K.; Borch, T.; Larese-Casanova, P.; Kappler, A., Redox Transformation of Arsenic by Fe(II)-Activated Goethite (α-FeOOH). *Environmental Science & Technology* **2010,** *44*, (1), 102-108.
9. Rosso, K. M.; Yanina, S. V.; Gorski, C. A.; Larese-Casanova, P.; Scherer, M. M., Connecting Observations of Hematite (α-Fe2O3) Growth Catalyzed by Fe(II). *Environmental Science & Technology* **2010,** *44*, (1), 61-67.
10. Latta, D. E.; Bachman, J. E.; Scherer, M. M., Fe Electron Transfer and Atom Exchange in Goethite: Influence of Al-Substitution and Anion Sorption. *Environmental Science & Technology* **2012,** *46*, (19), 10614-10623.
11. Neumann, A.; Olson, T. L.; Scherer, M. M., Spectroscopic Evidence for Fe(II)–Fe(III) Electron Transfer at Clay Mineral Edge and Basal Sites. *Environmental Science & Technology* **2013,** *47*, (13), 6969-6977.
12. Pasakarnis, T.; McCormick, M. L.; Parkin, G. F.; Thompson, A.; Scherer, M. M., Fe^{II}aq–Fe^{III}oxide electron transfer and Fe exchange: effect of organic carbon. *Environmental Chemistry* **2015,** *12*, (1), 52-63.
13. Latta, D. E.; Neumann, A.; Premaratne, W. A. P. J.; Scherer, M. M., Fe(II)–Fe(III) Electron Transfer in a Clay Mineral with Low Fe Content. *ACS Earth and Space Chemistry* **2017,** *1*, (4), 197-208.
14. Gorski, C. A.; Scherer, M. M., Influence of Magnetite Stoichiometry on Fe^{II} Uptake and Nitrobenzene Reduction. *Environmental Science & Technology* **2009,** *43*, (10), 3675-3680.
15. Schaefer, M. V.; Gorski, C. A.; Scherer, M. M., Spectroscopic Evidence for Interfacial Fe(II)−Fe(III) Electron Transfer in a Clay Mineral. *Environmental Science & Technology* **2011,** *45*, (2), 540-545.
16. Handler, R. M.; Beard, B. L.; Johnson, C. M.; Scherer, M. M., Atom Exchange between Aqueous Fe(II) and Goethite: An Fe Isotope Tracer Study. *Environmental Science & Technology* **2009,** *43*, (4), 1102-1107.

17. Handler, R. M.; Frierdich, A. J.; Johnson, C. M.; Rosso, K. M.; Beard, B. L.; Wang, C.; Latta, D. E.; Neumann, A.; Pasakarnis, T.; Premaratne, W. A. P. J.; Scherer, M. M., Fe(II)-Catalyzed Recrystallization of Goethite Revisited. *Environmental Science & Technology* **2014,** *48*, (19), 11302-11311.
18. Latta, Drew E.; Gorski, Christopher A.; Scherer, Michelle M., Influence of Fe^{2+}-catalysed iron oxide recrystallization on metal cycling. *Biochemical Society Transactions* **2012,** *40*, (6), 1191-1197.
19. Gorski, C. A.; Fantle, M. S., Stable mineral recrystallization in low temperature aqueous systems: A critical review. *Geochimica et Cosmochimica Acta* **2017,** *198*, 439-465.
20. Joshi, P.; Fantle, M. S.; Larese-Casanova, P.; Gorski, C. A., Susceptibility of Goethite to Fe^{2+}-Catalyzed Recrystallization over Time. *Environmental Science & Technology* **2017**.
21. Joshi, P.; Gorski, C. A., Anisotropic Morphological Changes in Goethite during Fe^{2+}-Catalyzed Recrystallization. *Environmental Science & Technology* **2016,** *50*, (14), 7315-7324.
22. Neumann, A.; Wu, L.; Li, W.; Beard, B. L.; Johnson, C. M.; Rosso, K. M.; Frierdich, A. J.; Scherer, M. M., Atom Exchange between Aqueous Fe(II) and Structural Fe in Clay Minerals. *Environmental Science & Technology* **2015,** *49*, (5), 2786-2795.
23. Gorski, C. A.; Handler, R. M.; Beard, B. L.; Pasakarnis, T.; Johnson, C. M.; Scherer, M. M., Fe Atom Exchange between Aqueous Fe^{2+} and Magnetite. *Environmental Science & Technology* **2012,** *46*, (22), 12399-12407.
24. Murray, G. C.; Hesterberg, D., Iron and phosphate dissolution during abiotic reduction of ferrihydrite-boehmite mixtures. *Soil Sci. Soc. Am. J.* **2006,** *70*, (4), 1318-1327.
25. Matocha, C. J.; Dhakal, P.; Pyzola, S. M., Chapter Four - The Role of Abiotic and Coupled Biotic/Abiotic Mineral Controlled Redox Processes in Nitrate Reduction. In *Advances in Agronomy*, Donald, L. S., Ed. Academic Press: 2012; Vol. Volume 115, pp 181-214.
26. Van Cleemput, O., Subsoils: chemo-and biological denitrification, N_2O and N_2 emissions. *Nutrient Cycling in Agroecosystems* **1998,** *52*, (2-3), 187-194.
27. Ernstsen, V., Reduction of Nitrate by Fe^{2+} in Clay Minerals. *Clays and Clay Minerals* **1996,** *44*, (5), 599-608.
28. Colombo, C.; Palumbo, G.; He, J.-Z.; Pinton, R.; Cesco, S., Review on iron availability in soil: interaction of Fe minerals, plants, and microbes. *Journal of Soils and Sediments* **2014,** *14*, (3), 538-548.
29. Weber, K. A.; Achenbach, L. A.; Coates, J. D., Microorganisms pumping iron: anaerobic microbial iron oxidation and reduction. *Nat Rev Micro* **2006,** *4*, (10), 752-764.
30. Chun, C. L.; Hozalski, R. M.; Arnold, W. A., Degradation of Drinking Water Disinfection Byproducts by Synthetic Goethite and Magnetite. *Environmental Science & Technology* **2005,** *39*, (21), 8525-8532.
31. Peretyazhko, T.; Zachara, J. M.; Heald, S. M.; Jeon, B. H.; Kukkadapu, R. K.; Liu, C.; Moore, D.; Resch, C. T., Heterogeneous reduction of Tc(VII) by Fe(II) at the solid–water interface. *Geochimica et Cosmochimica Acta* **2008,** *72*, (6), 1521-1539.
32. Latta, D. E.; Boyanov, M. I.; Kemner, K. M.; O'Loughlin, E. J.; Scherer, M. M., Abiotic reduction of uranium by Fe (II) in soil. *Applied geochemistry* **2012,** *27*, (8), 1512-1524.
33. Stemig, A. M.; Do, T. A.; Yuwono, V. M.; Arnold, W. A.; Penn, R. L., Goethite nanoparticle aggregation: effects of buffers, metal ions, and 4-chloronitrobenzene reduction. *Environmental Science: Nano* **2014,** *1*, (5), 478-487.

34. Tomaszewski, E. J.; Lee, S.; Rudolph, J.; Xu, H.; Ginder-Vogel, M., The reactivity of Fe(II) associated with goethite formed during short redox cycles toward Cr(VI) reduction under oxic conditions. *Chemical Geology* **2017,** *464*, 101-109.
35. Frierdich, A. J.; Catalano, J. G., Fe(II)-Mediated Reduction and Repartitioning of Structurally Incorporated Cu, Co, and Mn in Iron Oxides. *Environmental Science & Technology* **2012,** *46*, (20), 11070-11077.
36. Pedersen, H. D.; Postma, D.; Jakobsen, R.; Larsen, O., Fast transformation of iron oxyhydroxides by the catalytic action of aqueous Fe(II). *Geochimica et Cosmochimica Acta* **2005,** *69*, (16), 3967-3977.
37. Johnson, C. M.; Beard, B. L.; Roden, E. E., The Iron Isotope Fingerprints of Redox and Biogeochemical Cycling in Modern and Ancient Earth. *Annual Review of Earth and Planetary Sciences* **2008,** *36*, (1), 457-493.
38. Alexandrov, V.; Rosso, K. M., Ab initio modeling of Fe(II) adsorption and interfacial electron transfer at goethite (α-FeOOH) surfaces. *Physical Chemistry Chemical Physics* **2015,** *17*, (22), 14518-14531.
39. Kubicki, J. D.; Tunega, D.; Kraemer, S., A density functional theory investigation of oxalate and Fe(II) adsorption onto the (010) goethite surface with implications for ligand- and reduction-promoted dissolution. *Chemical Geology* **2016**.
40. Russell, B.; Payne, M.; Ciacchi, L. C., Density functional theory study of Fe(II) adsorption and oxidation on goethite surfaces. *Physical Review B* **2009,** *79*, (16), 165101.
41. Zarzycki, P.; Kerisit, S.; Rosso, K. M., Molecular Dynamics Study of Fe(II) Adsorption, Electron Exchange, and Mobility at Goethite (α-FeOOH) Surfaces. *The Journal of Physical Chemistry C* **2015,** *119*, (6), 3111-3123.
42. Soltis, J. A.; Schwartzberg, A. M.; Zarzycki, P.; Penn, R. L.; Rosso, K. M.; Gilbert, B., Electron Mobility and Trapping in Ferrihydrite Nanoparticles. *ACS Earth and Space Chemistry* **2017,** *1*, (4), 216-226.
43. Schwertmann, U.; Cambier, P.; Murad, E., Properties of goethites of varying crystallinity. *Clays and Clay minerals* **1985,** *33*, (5), 369-378.
44. Strauss, R.; Brümmer, G. W.; Barrow, N. J., Effects of crystallinity of goethite: I. Preparation and properties of goethites of differing crystallinity. *European Journal of Soil Science* **1997,** *48*, (1), 87-99.
45. Madsen, D. E.; Cervera-Gontard, L.; Kasama, T.; Dunin-Borkowski, R. E.; Koch, C. B.; Hansen, M. F.; Frandsen, C.; Mørup, S., Magnetic fluctuations in nanosized goethite (α-FeOOH) grains. *Journal of Physics: Condensed Matter* **2009,** *21*, (1), 016007.
46. Barrero, C. A.; Betancur, J. D.; Greneche, J. M.; Goya, G. F.; Berquó, T. S., Magnetism in non-stoichiometric goethite of varying total water content and surface area. *Geophysical Journal International* **2006,** *164*, (2), 331-339.
47. Bocquet, S.; Hill, A., Correlation of Néel temperature and vacancy defects in fine-particle goethites. *Physics and Chemistry of Minerals* **1995,** *22*, (8), 524-528.
48. Cornell, R. M.; Schwertmann, U., Crystal Structure. In *The Iron Oxides*, Wiley-VCH Verlag GmbH & Co. KGaA: 2004; pp 9-38.
49. De Yoreo, J. J.; Gilbert, P. U.; Sommerdijk, N. A.; Penn, R. L.; Whitelam, S.; Joester, D.; Zhang, H.; Rimer, J. D.; Navrotsky, A.; Banfield, J. F., Crystallization by particle attachment in synthetic, biogenic, and geologic environments. *Science* **2015,** *349*, (6247), aaa6760.
50. Penn, R. L.; Banfield, J. F., Imperfect Oriented Attachment: Dislocation Generation in Defect-Free Nanocrystals. *Science* **1998,** *281*, (5379), 969-971.

51. Banfield, J. F.; Welch, S. A.; Zhang, H.; Ebert, T. T.; Penn, R. L., Aggregation-Based Crystal Growth and Microstructure Development in Natural Iron Oxyhydroxide Biomineralization Products. *Science* **2000,** *289*, (5480), 751-754.
52. Brož, D.; Sedlák, B., Surface ferrimagnetism of synthetic goethite. *Journal of Magnetism and Magnetic Materials* **1991,** *102*, (1), 103-108.
53. Bocquet, S.; Pollard, R. J.; Cashion, J. D., Dynamic magnetic phenomena in fine-particle goethite. *Physical Review B* **1992,** *46*, (18), 11657-11664.
54. Stacey, F. D.; Banerjee, S. K., Chapter 2 - Magnetic Minerals. In *Developments in Solid Earth Geophysics*, Frank D, S.; Subir K, B., Eds. Elsevier: 1974; Vol. Volume 5, pp 25-40.
55. Özdemir, Ö.; Dunlop, D. J., Thermoremanence and Néel temperature of goethite. *Geophysical Research Letters* **1996,** *23*, (9), 921-924.
56. Fischer, L.; Mühlen, E. Z.; Brümmer, G. W.; Niehus, H., Atomic force microscopy (AFM) investigations of the surface topography of a multidomain porous goethite. *European Journal of Soil Science* **1996,** *47*, (3), 329-334.
57. Schwertmann, U.; Cornell, R. M., Goethite. In *Iron Oxides in the Laboratory*, Wiley-VCH Verlag GmbH: 2007; pp 67-92.
58. Good, N. E.; Winget, G. D.; Winter, W.; Connolly, T. N.; Izawa, S.; Singh, R. M. M., Hydrogen Ion Buffers for Biological Research*. *Biochemistry* **1966,** *5*, (2), 467-477.
59. Tamura, H.; Goto, K.; Yotsuyanagi, T.; Nagayama, M., Spectrophotometric determination of iron(II) with 1,10-phenanthroline in the presence of large amounts of iron(III). *Talanta* **1974,** *21*, (4), 314-318.
60. Rancourt, D. G.; Ping, J. Y., Voigt-based methods for arbitrary-shape static hyperfine parameter distributions in Mössbauer spectroscopy. *Nuclear Instruments and Methods in Physics Research Section B: Beam Interactions with Materials and Atoms* **1991,** *58*, (1), 85-97.
61. Joly, Y., X-ray absorption near-edge structure calculations beyond the muffin-tin approximation. *Physical Review B* **2001,** *63*, (12), 125120.
62. Hedin, L.; Lundqvist, B. I., Explicit local exchange-correlation potentials. *Journal of Physics C: Solid State Physics* **1971,** *4*, (14), 2064.
63. Piepenbrock, A.; Schröder, C.; Kappler, A., Electron transfer from humic substances to biogenic and abiogenic Fe (III) oxyhydroxide minerals. *Environmental science & technology* **2014,** *48*, (3), 1656-1664.
64. Buchholz, A.; Laskov, C.; Haderlein, S. B., Effects of Zwitterionic Buffers on Sorption of Ferrous Iron at Goethite and Its Oxidation by CCl4. *Environmental Science & Technology* **2011,** *45*, (8), 3355-3360.
65. Cornell, R. M.; Schwertmann, U., Formation. In *The Iron Oxides*, Wiley-VCH Verlag GmbH & Co. KGaA: 2004; pp 345-364.
66. Burns, R. G., Intervalence transitions in mixed valence minerals of iron and titanium. *Annual Review of Earth and Planetary Sciences* **1981,** *9*, (1), 345-383.
67. Liu, J.; Pearce, C. I.; Liu, C.; Wang, Z.; Shi, L.; Arenholz, E.; Rosso, K. M., $Fe_{3-x}Ti_xO_4$ Nanoparticles as Tunable Probes of Microbial Metal Oxidation. *Journal of the American Chemical Society* **2013,** *135*, (24), 8896-8907.
68. Sassi, M.; Pearce, C. I.; Bagus, P. S.; Arenholz, E.; Rosso, K. M., First Principles Fe $L_{2,3}$-Edge and O K-Edge XANES and XMCD Spectra for Iron Oxides. *The Journal of Physical Chemistry A* **2017**.
69. Gilbert, B.; Erbs, J. J.; Penn, R. L.; Petkov, V.; Spagnoli, D.; Waychunas, G. A., A disordered nanoparticle model for 6-line ferrihydrite. *American Mineralogist* **2013,** *98*, (8-9), 1465-1476.

70. Frierdich, A. J.; Catalano, J. G., Controls on Fe(II)-Activated Trace Element Release from Goethite and Hematite. *Environmental Science & Technology* **2012,** *46*, (3), 1519-1526.
71. Jones, A. M.; Collins, R. N.; Rose, J.; Waite, T. D., The effect of silica and natural organic matter on the Fe(II)-catalysed transformation and reactivity of Fe(III) minerals. *Geochimica et Cosmochimica Acta* **2009,** *73*, (15), 4409-4422.
72. Frierdich, A. J.; Helgeson, M.; Liu, C.; Wang, C.; Rosso, K. M.; Scherer, M. M., Iron atom exchange between hematite and aqueous Fe(II). *Environmental science & technology* **2015,** *49*, (14), 8479-8486.
73. Roden, E. E.; Urrutia, M. M.; Mann, C. J., Bacterial Reductive Dissolution of Crystalline Fe(III) Oxide in Continuous-Flow Column Reactors. *Applied and Environmental Microbiology* **2000,** *66*, (3), 1062-1065.
74. Roden, E. E.; Urrutia, M. M., Influence of biogenic Fe (II) on bacterial crystalline Fe (III) oxide reduction. *Geomicrobiology journal* **2002,** *19*, (2), 209-251.
75. Klausen, J.; Trober, S. P.; Haderlein, S. B.; Schwarzenbach, R. P., Reduction of substituted nitrobenzenes by Fe(II) in aqueous mineral suspensions. *Environmental Science and Technology* **1995,** *29*, (9), 2396-2404.
76. Amonette, J. E.; Workman, D. J.; Kennedy, D. W.; Fruchter, J. S.; Gorby, Y. A., Dechlorination of carbon tetrachloride by Fe(II) associated with goethite. *Environmental Science & Technology* **2000,** *34*, (21), 4606-4613.
77. Gorski, C. A.; Edwards, R.; Sander, M.; Hofstetter, T. B.; Stewart, S. M., Thermodynamic Characterization of Iron Oxide–Aqueous Fe^{2+} Redox Couples. *Environmental Science & Technology* **2016,** *50*, (16), 8538-8547.
78. Fan, D.; Bradley, M. J.; Hinkle, A. W.; Johnson, R. L.; Tratnyek, P. G., Chemical Reactivity Probes for Assessing Abiotic Natural Attenuation by Reducing Iron Minerals. *Environmental Science & Technology* **2016,** *50*, (4), 1868-1876.
79. Wang, L.; Giammar, D. E., Effects of pH, dissolved oxygen, and aqueous ferrous iron on the adsorption of arsenic to lepidocrocite. *Journal of colloid and interface science* **2015,** *448*, 331-338.
80. Ilgen, A. G.; Kruichak, J.; Artyushkova, K.; Newville, M.; Sun, C.-J., Redox transformations of As and Se at the surfaces of natural and synthetic ferric nontronites: role of structural and adsorbed Fe(II). *Environmental Science & Technology* **2017**.

Supporting Information

The Role of Defects in Fe(II)-Goethite Electron Transfer

Luiza Notini[1], Drew E. Latta[1], Anke Neumann[2], Carolyn I. Pearce[3], Michel Sassi[3], Alpha T. N'Diaye[4], Kevin M. Rosso[3], and Michelle Scherer[1,*]

[1]Department of Civil and Environmental Engineering, University of Iowa, Iowa City, IA, 52242, United States.
[2]School of Engineering, Newcastle University, Newcastle upon Tyne, NE1 7RU, United Kingdom.
[3]Pacific Northwest National Laboratory, Richland, WA 99352, United States
[4]Advanced Light Source, Lawrence Berkeley National Laboratory, Berkeley, CA 94720

Figures: 12

Tables: 3

Pages: 22

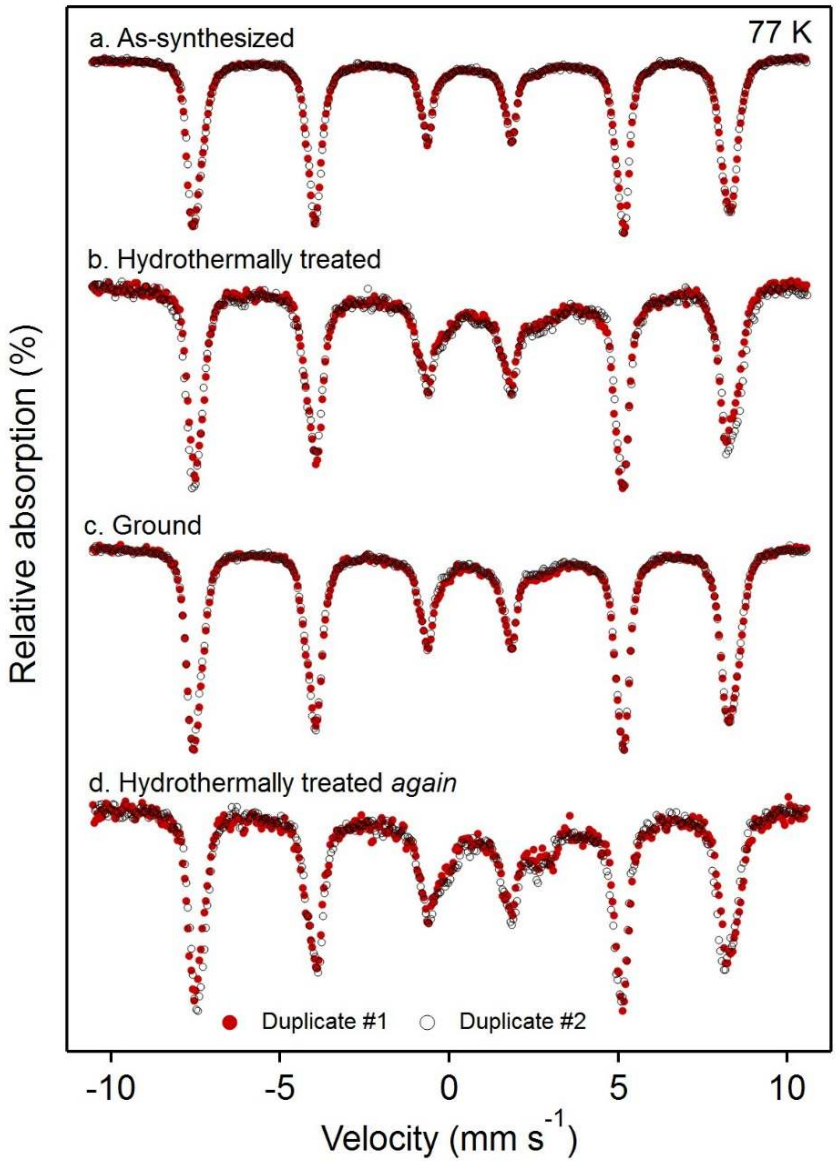

Figure S1. Mössbauer spectra of 1 mM ^{57}Fe(II) reacted with goethite after sequential hydrothermal/grinding treatments. Different colors represent different batches.

Fitting Mössbauer spectra

We tried different approaches to fit the spectral area not captured by the two goethite sextets. In the first approach we used a doublet as in some of our and others' work.[1, 2] This fitting procedure, however, does not capture any area in the ranges of -4 to -1 and 4 to 5 mm s^{-1}. In the second approach we added a doublet and a broad, partially order collapsed feature, as in our previous work (**Figure S2**).[3] We qualitatively concluded based on visual inspection of multiple fits that the doublet along with collapsed sextet is the best approach. Our qualitative analysis is quantitatively supported by a smaller χ^2 values calculated when the collapsed sextet was included.

To model the collapsed feature parameters, we attempted to fit the spectrum by inputting a wide range of center shifts (from 0.1 to 1.7 mm s^{-1}). The parameters converged to two stable solutions, with center shifts of ≈0.65 or ≈1.3 mm s^{-1}. A center shift ≈1.3 mm s^{-1} would be an indication of an Fe(II) compound, however the presence of ferrous hydroxide can be ruled out by XRD (**Figure S3**) and based on our observation of a high hyperfine field of 25 T, compared to absence of magnetic ordering for ferrous hydroxide at 77 K (doublet parameter: CS = 1.21 mm s^{-1}; QS = 2.95 mm s^{-1}).[4] For that reason we chose to fit our spectra using the center shift of 0.65 mm s^{-1}, as this value would be reasonable for a mixed Fe(II)-Fe(III) compound.[5] We also collected Mössbauer data at 4 K, which showed no indication of magnetic ordering, ruling out the presence well-defined mineral Fe(II)-Fe(III) compounds (e.g., green rust). More importantly though, neither the relative area of the components nor the remaining parameters of the sextets seem to be substantially affected by the two different center shifts. Thereby, we limited our interpretation to suggest that the collapsed feature is a non-well defined Fe(II)-Fe(III) compound, and we used the fitting of the Mössbauer spectra to calculate the relative area of the component.

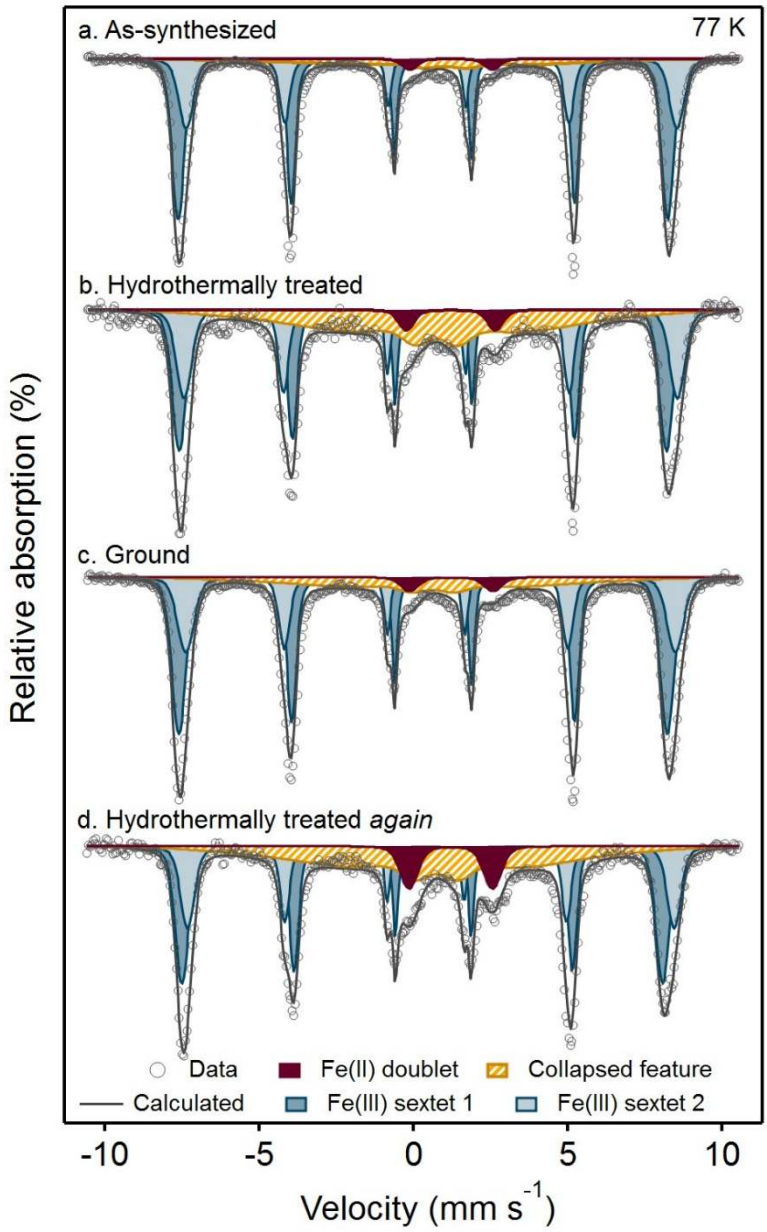

Figure S2. Mössbauer spectra of 1 mM ^{57}Fe(II) reacted with goethite after sequential hydrothermal/grinding treatments. Experimental conditions: [^{56}Gt]= 2 g L^{-1} ; 1 mM Fe(II) in 25 mM KBr/25 mM HEPES at pH 7.5.

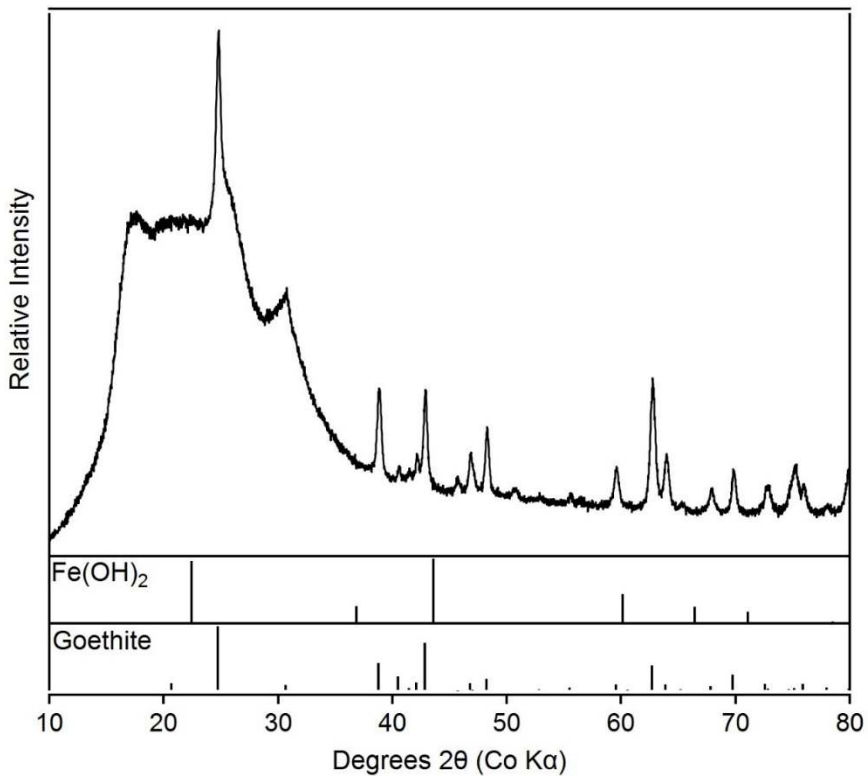

Figure S3. Power X-ray diffraction of ^{56}Fe as-synthesized goethite reacted with 1mM $^{57}Fe(II)$. Sample was filtered and protected against oxidation with Kapton tape.

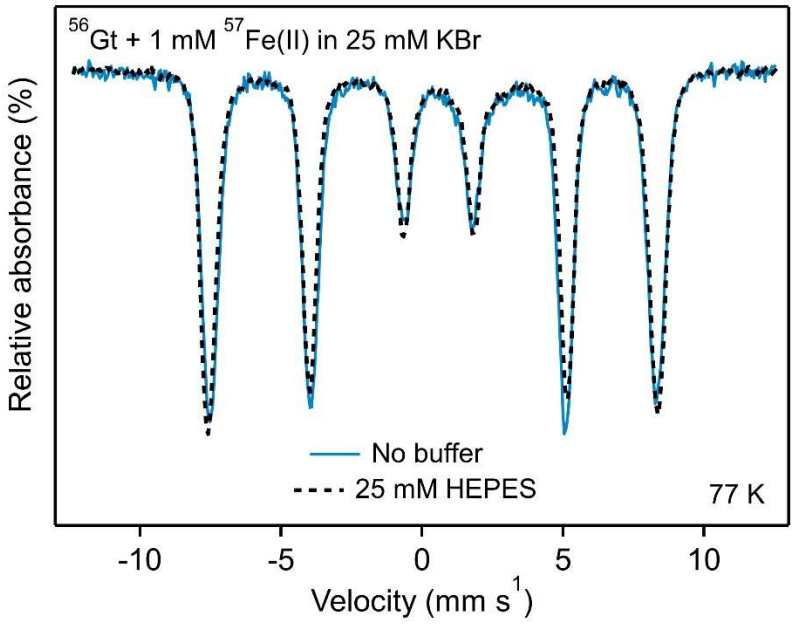

Figure S4. Mössbauer spectra of ^{56}goethite reacted with 1 mM ^{57}Fe(II) in the presence and in the absence of 25 mM HEPES. Experimental conditions: [^{56}Gt]= 2 g L^{-1}; 25 mM KBr; initial pH 7.5.

Mössbauer spectra of extracted and oxidized samples

In order to determine what is removed from the reacted solids upon acid extractions or air oxidation, we compared the spectra of the HCl extracted goethite and oxidized goethite (**Figure 2**). The oxidation of the sample revealed the complete removal of the Fe(II) doublet and the collapsed feature and we hypothesize that this is due to the Fe(II) content on these features. The spectrum contains two sextets (CS ≈ 0.48 mm s^{-1}, QS ≈ -0.16 mm s^{-1} and CS ≈ 0.5 mm s^{-1}, QS ≈ 0.08 mm s^{-1}) as was observed after reaction of goethite with ^{57}Fe(II) (**Table S1**). To rule out aging as a factor in removing the doublet and collapsed feature we left one sample inside the glovebox where it was not exposed to oxygen and the collapsed feature and Fe(II) remained (data not shown).

In contrast, the HCl-extracted goethite spectrum clearly has a third Fe(III) sextet. The Mössbauer parameters of the third Fe(III) sextet (**Table S1**) are similar to those reported for akaganéite (β - FeOOH),[6] and we hypothesize akaganéite was formed due to the extractant's chloride content and low pH value.

To confirm that the formation of akaganéite was due to the acid extraction, we then tried a mild sequential extraction with buffer (pH 7.5, 1 hour) followed by 1 M $CaCl_2$ (pH 7, 4 hours) and 1 M NaH_2PO_4 (pH 5, 18 hours). A 30 min wash step with DI water was carried out after the $CaCl_2$ and NaH_2PO_4. The Mössbauer spectrum of the extracted solids (**Figure S5**) showed removal of most of the collapsed feature (**Table S1**), and 80% of sorbed Fe(II) was recovered during the sequential extractions (**Table S2**). In contrast to the spectrum of the HCl-extracted goethite, the Mössbauer spectrum of the sequentially extracted solids did not contain a third sextet. The appearance of the third sextet after the HCl extraction and its absence after the sequential extraction further suggests the component is a result of the acidic pH value and the high chloride content of the extraction solution, and did not result from the removal of Fe(II).

Taken together the extraction and oxidation treatments confirm that removal of Fe(II) is concomitant with the loss of the collapsed feature, and provides a line of evidence that the collapsed feature, at least in part, arises from the presence of Fe(II) in the solids formed during the electron transfer from Fe(II) to goethite.

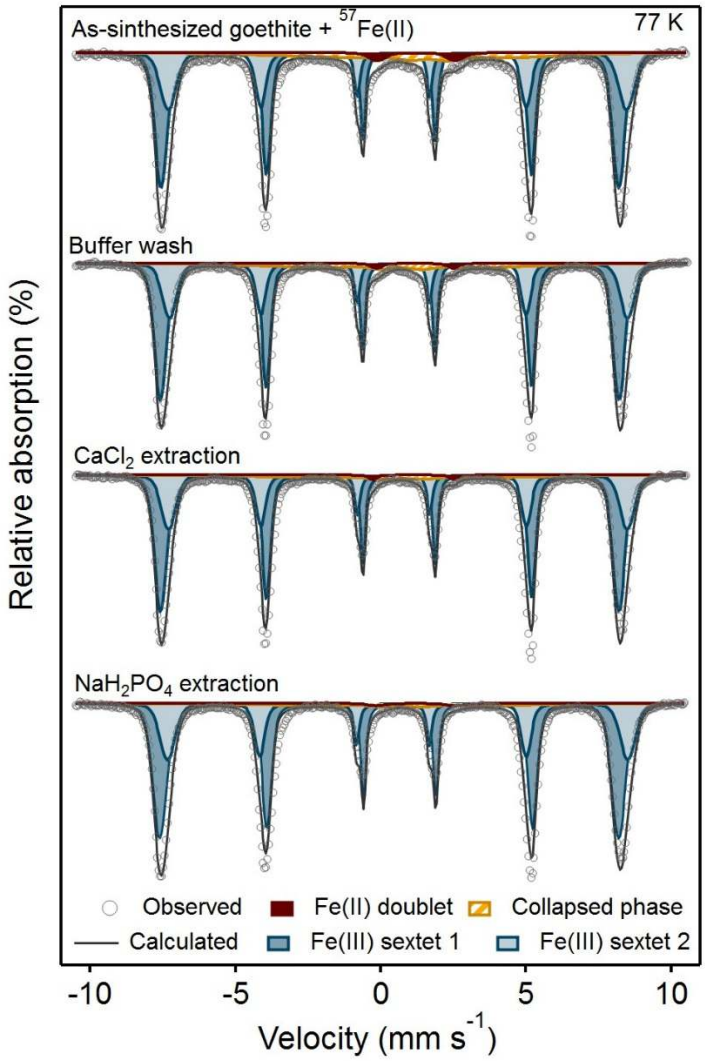

Figure S5. Mössbauer spectra of ^{56}Fe as-synthesized goethite reacted with 1 mM ^{57}Fe(II), before and after sequential buffer wash and 1 M $CaCl_2$ and NaH_2PO_4 extraction.

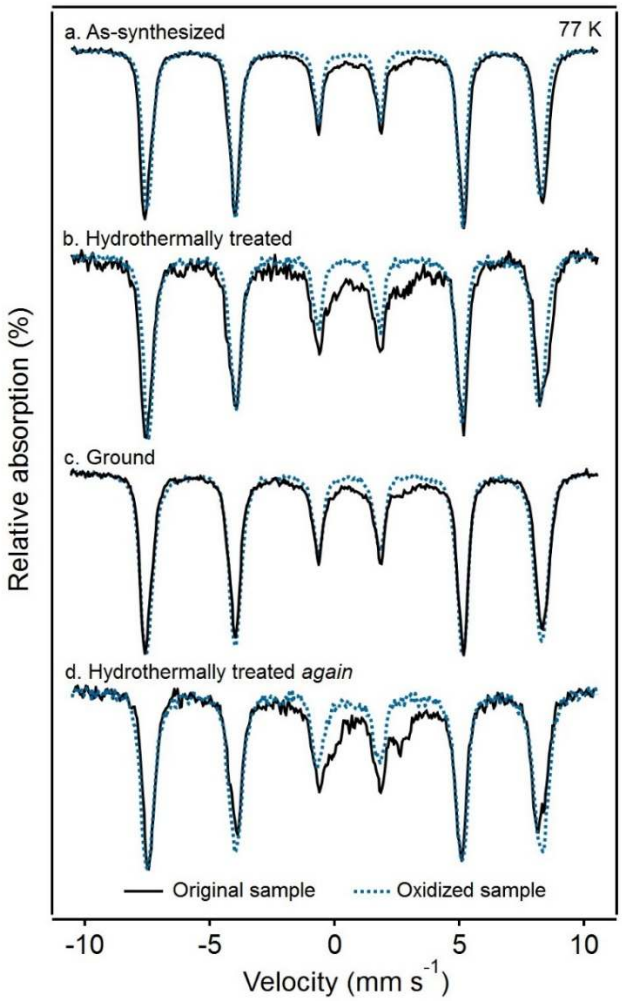

Figure S6. Mössbauer spectra of 1 mM ^{57}Fe(II) reacted with goethite after sequential hydrothermal/grinding treatments, before (original: solid lines) and after oxidation (oxidized: dotted lines).

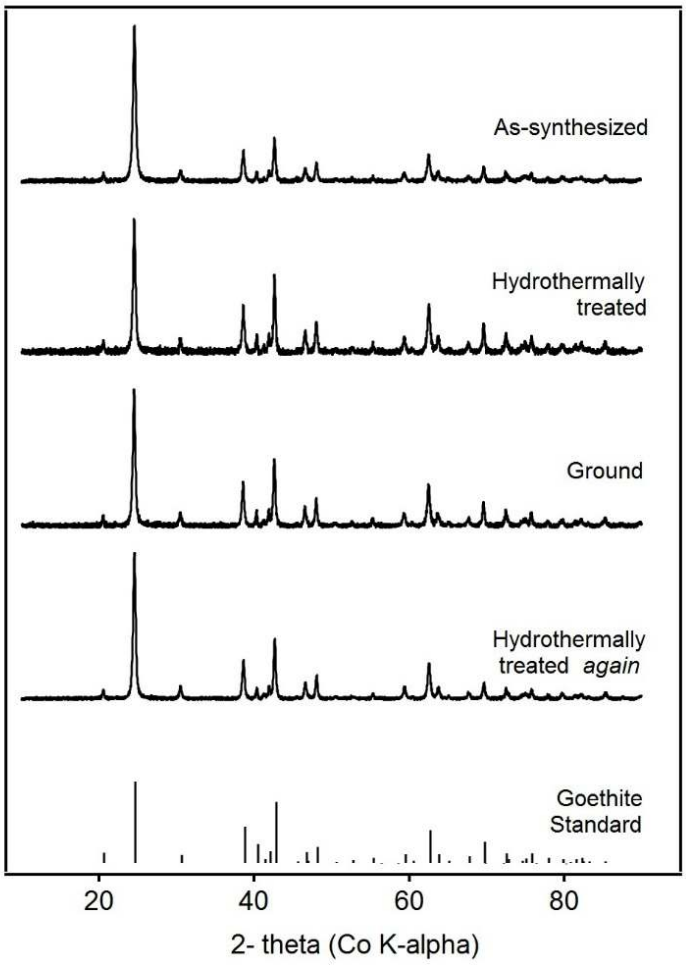

Figure S7. XRD of goethite after sequential hydrothermal/grinding treatments.

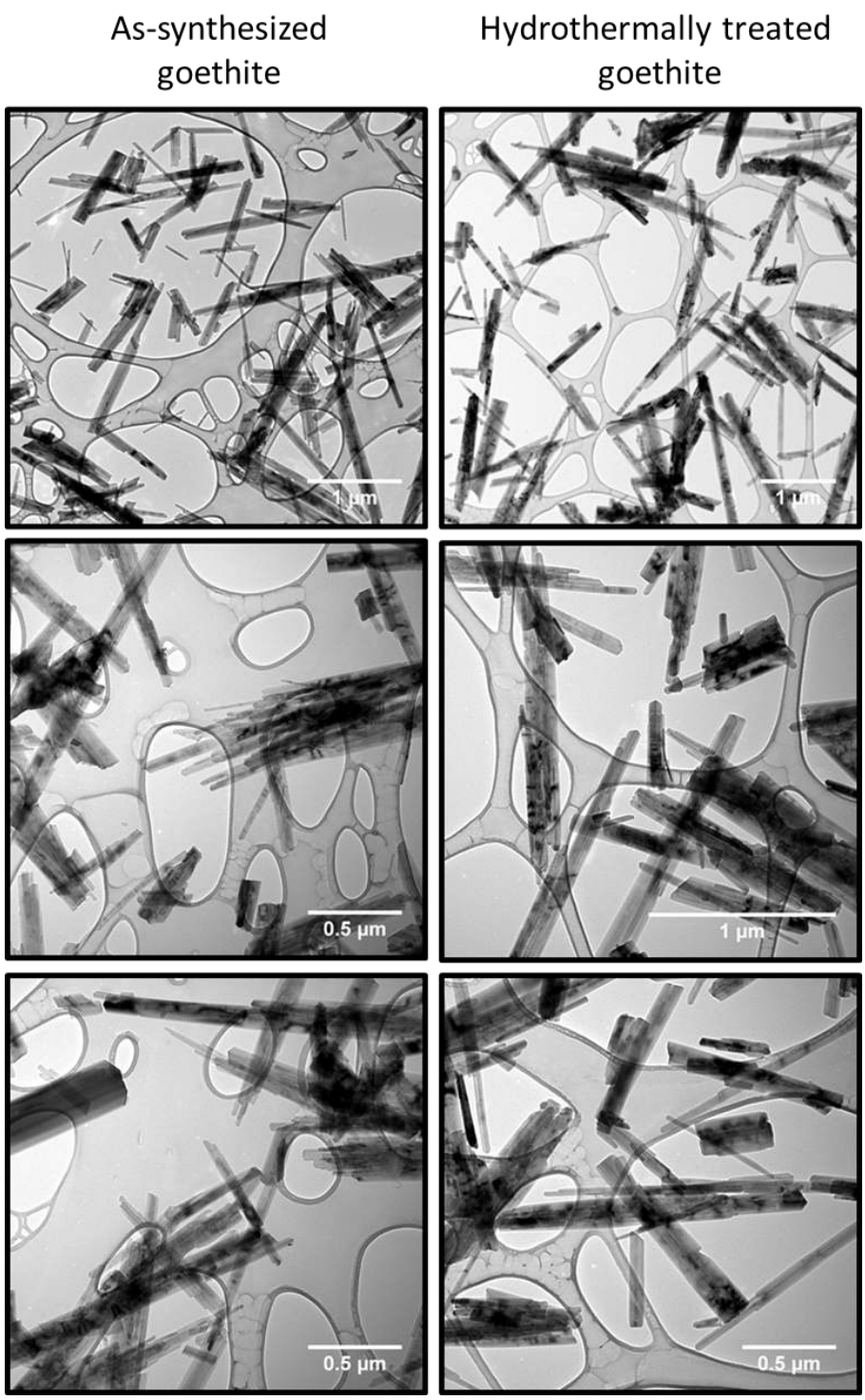

Figure S8. TEM picture of as-synthesized goethite and hydrothermally treated goethite.

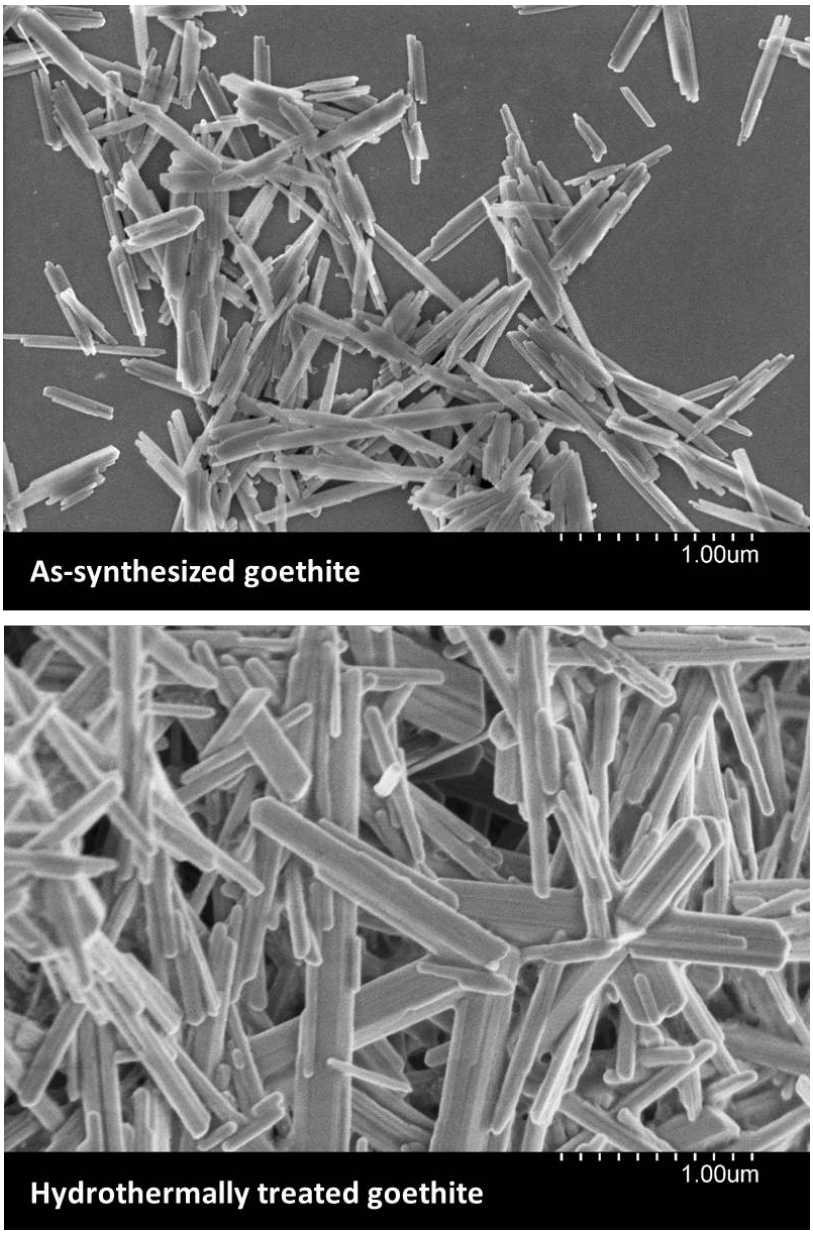

Figure S9. SEM picture of as-synthesized goethite and hydrothermally treated goethite.

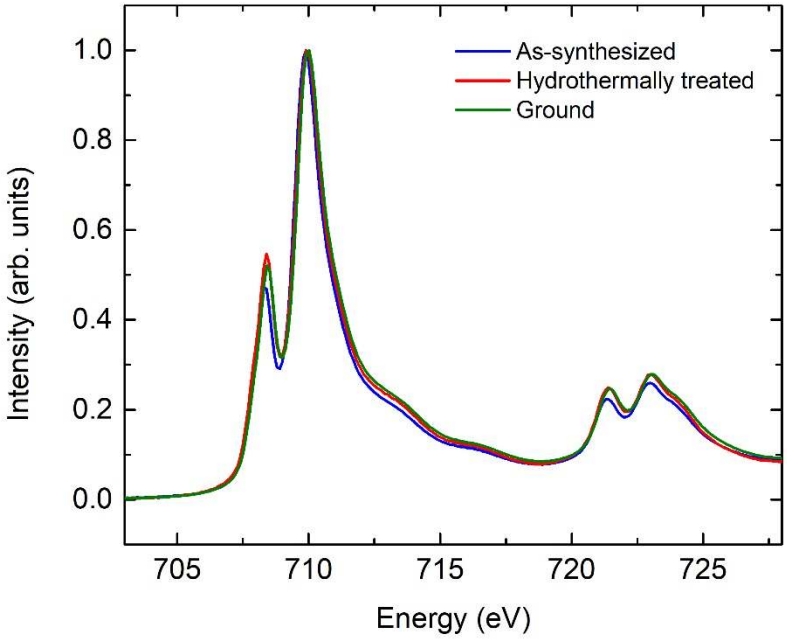

Figure S10. Fe L-edge XAS of goethite after sequential hydrothermal/grinding treatments.

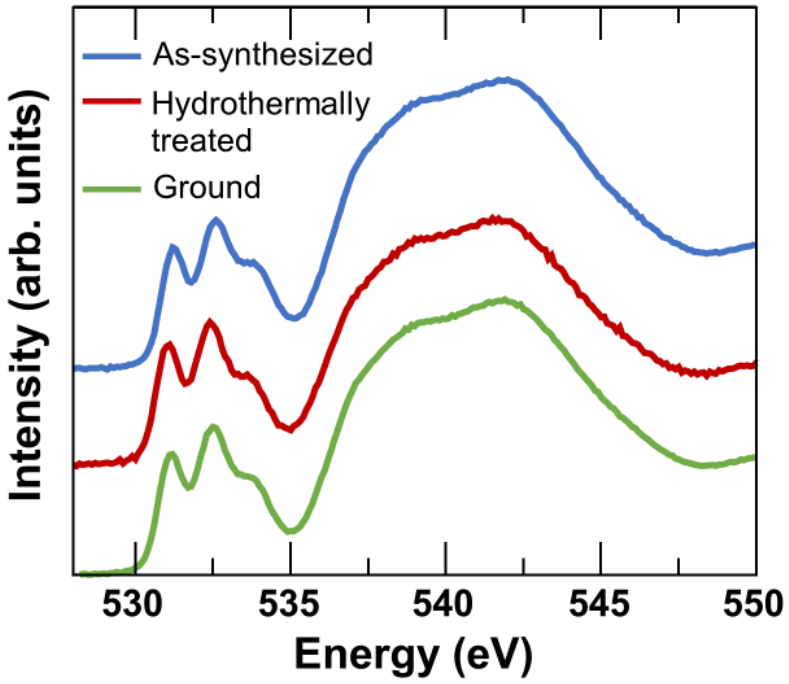

Figure S11. O K-edge XAS of goethite after sequential hydrothermal/grinding treatments.

Calculated linear combination fit of O K-edge XANES spectra

In goethite there are two different environments for the oxygen atoms such that one of the oxygen sites is bounded to three iron atoms, while the other is in a tetrahedral site, linked to three iron atoms and one hydrogen atom. The two oxygen sites are involved in an O···H—O hydrogen bond interaction with each other. The oxygen site linked to a hydrogen atom will be referred as "OH", while the other will be referred as "O". We used the linear combination of these two theoretically calculated contributions to reproduce the experimental O K-edge spectra of goethite samples under different experimental conditions.

Figure S12a shows that a good agreement can be obtained between the experimental spectra and the linear combination (LC) of the O K-edge spectra from the two oxygen sites. Especially, the intensity ratio between the peaks 2 and 3 in the calculated LC are very well reproduced for each case. **Figures S12(c-e)** show that the spectra from the O site are the main contributions to the lower energy peaks 1 and 2, while the OH site is the dominant contribution to the higher energy peak 3. For the as-synthesized goethite, shown in **Figure S12c**, the calculated relative area contribution from O and OH sites is 52.5% and 47.5% respectively, which is in good agreement with previous work[7] using a doublet composed of two Gaussian functions for the O and OH components to reproduce the experimental spectra of goethite, and not too far away from the ideal 50% for each site type.

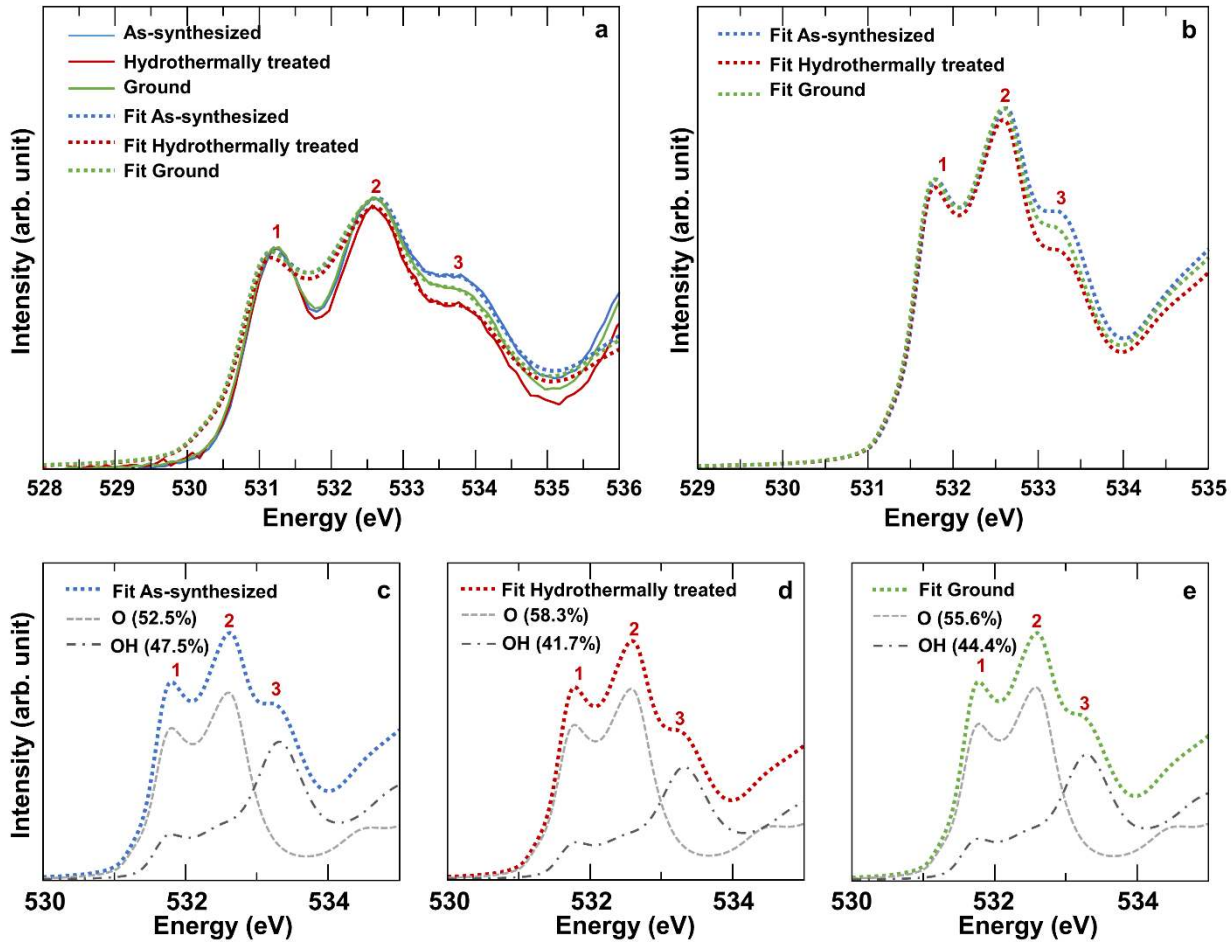

Figure S12. (a) Comparison between experimental goethite samples and calculated O K-edge spectra obtained by linear combination (LC) of O and OH components. The spectra have been linearly expanded in energy to allow a better comparison with the experimental spectra. (b) Unmodified calculated O K-edge spectra from linear combination. (c-e) Individual O and OH components in the linear combination of each case considered.

Table S1. Mössbauer parameters derived from fitting spectra collected at 77 K for 1 mM ^{57}Fe(II) reacted with goethite after sequential hydrothermal/grinding treatments in addition to oxidized and HCl-extracted samples.

Sample	Experiment		Mössbauer parameters					
			Component	CS[a] (mm s^{-1})	QS[b] (mm s^{-1})	H[c] (Tesla)	Std(H) or Std(QS)[d] (Tesla) or (mm s^{-1})	Area (%)
^{56}Fe As-synthesized goethite + 1mM ^{57}Fe(II)	**Batch #**	2	**Fe(II)**	1.17	2.68		0.35	2.2
	Initial Fe(II)	1.15 mM	**Fe(III) Sextet 1**	0.47	-0.16	49.0	1.02	59.1
	Sorbed Fe(II)	188 μmoles g^{-1}	**Fe(III) Sextet 2**	0.51	0.07	49.0	1.29	29.6
	Rel. Area sextets	88.7%	**Collapsed Feature**	0.65[e]	-0.10[e]	25.8[e]	14.65[e]	9.2
	Batch #	3	**Fe(II)**	1.22	2.62		0.41	2.0
	Initial Fe(II)	1.063 mM	**Fe(III) Sextet 1**	0.48	-0.16	49.1	0.94	56.7
	Sorbed Fe(II)	139 μmoles g^{-1}	**Fe(III) Sextet 2**	0.51	0.07	49.3	1.19	29.1
	Rel. Area sextets	85.8%	**Collapsed Feature**	0.65[e]	-0.10[e]	25.8[e]	14.65[e]	12.2
	Oxidized sample		**Fe(III) Sextet 1**	0.47	-0.17	48.6	0.91	61.9
	Rel. Area sextets	100.0%	**Fe(III) Sextet 2**	0.51	0.03	48.8	0.96	38.1
	After HCl extraction		**Fe(III) Sextet 1**	0.48	-0.15	48.3	0.90	45.4
			Fe(III) Sextet 2	0.50	0.06	48.5	0.99	29
	Rel. Area sextets	100.0%	**Fe(III) Sextet 3**	0.45	-0.37	47.1	0.95	25.5
	Sequential extractions Buffer wash		**Fe(II)**	1.18	2.63		0.28	1.0
			Fe(III) Sextet 1	0.48	-0.16	48.9	1.02	61.6
			Fe(III) Sextet 2	0.53	0.09	48.9	0.25	28.4
	Rel. Area sextets	90.0%	**Collapsed Feature**	0.65[e]	-0.10[e]	25.4[e]	13.23[e]	9.0
	Sequential extractions $CaCl_2$		**Fe(II)**	1.13	2.79		0.18	0.8
			Fe(III) Sextet 1	0.48	-0.16	48.9	1.04	63.4
			Fe(III) Sextet 2	0.52	0.07	49.0	1.27	29.1
	Rel. Area sextets	92.5%	**Collapsed Feature**	0.65[e]	-0.10[e]	25.8[e]	14.65[e]	6.7
	Sequential extractions NaH_2PO_4		**Fe(II)**	1.20[e]	2.70[e]		0.50[e]	0.6
			Fe(III) Sextet 1	0.48	-0.18	49	1.20	64.0
			Fe(III) Sextet 2	0.51	0.08[e]	49.1	1.35	30.5
	Rel. Area sextets	94.5%	**Collapsed Feature**	0.65[e]	-0.10[e]	25.4[e]	13.23[e]	4.8

Sample	Experiment		Mössbauer parameters					
			Component	CS[a] ($mm\ s^{-1}$)	QS[b] ($mm\ s^{-1}$)	H[c] (Tesla)	Std(H) or Std(QS)[d] (Tesla) or ($mm\ s^{-1}$)	Area (%)
^{56}Fe Hydrothermally treated goethite + 1mM ^{57}Fe(II)	**Batch #**	2	**Fe(II)**	1.17	2.78		0.35	2.4
	Initial Fe(II)	1.14 mM	**Fe(III) Sextet 1**	0.47	-0.17	48.7	1.01	41.2
	Sorbed Fe(II)	136 µmoles g^{-1}	**Fe(III) Sextet 2**	0.51	0.09	49.2	1.13	24.0
	Rel. Area sextets	65.2%	**Collapsed Feature**	0.65[e]	-0.10[e]	25.8[e]	14.65[e]	32.4
	Batch #	3	**Fe(II)**	1.21	2.88		0.41	3.1
	Initial Fe(II)	1.132 mM	**Fe(III) Sextet 1**	0.48	-0.17	48.9	1.10	39.4
	Sorbed Fe(II)	122 µmoles g^{-1}	**Fe(III) Sextet 2**	0.49	0.06	1.25	1.25	26.9
	Rel. Area sextets	66.3%	**Collapsed Feature**	0.65[e]	-0.10[e]	25.8[e]	14.65[e]	30.6
	Oxidized sample		**Fe(II)**	1.20	2.70		0.50	0.1
			Fe(III) Sextet 1	0.48	-0.17	48.3	1.06	55.8
			Fe(III) Sextet 2	0.48	0.04	48.7	1.21	36.6
	Rel. Area sextets	92.4%	**Collapsed Feature**	0.65[e]	-0.10[e]	25.8[e]	14.65[e]	7.5
^{56}Fe Ground goethite + 1mM ^{57}Fe(II)	**Batch #**	3	**Fe(II)**	1.22	2.81		0.49	3.1
	Initial Fe(II)	1.104 mM	**Fe(III) Sextet 1**	0.48	-0.16	49.0	1.13	51.8
	Sorbed Fe(II)	106 µmoles g^{-1}	**Fe(III) Sextet 2**	0.50	0.07	49.4	1.40	30.1
	Rel. Area sextets	81.9%	**Collapsed Feature**	0.65[e]	-0.1[e]	25.8[e]	14.65[e]	15.0
	Batch #	3	**Fe(II)**	1.22	2.70		0.53	3.2
	Initial Fe(II)	1.123 mM	**Fe(III) Sextet 1**	0.48	-0.17	48.9	1.13	48.9
	Sorbed Fe(II)	99	**Fe(III) Sextet 2**	0.49	0.07	49.4	1.39	31.0
	Rel. Area sextets	79.9%	**Collapsed Feature**	0.65[e]	-0.10[e]	25.8[e]	14.65[e]	16.9
	Oxidized sample		**Fe(III) Sextet 1**	0.48	-0.21	48.8	1.30	50.5
			Fe(III) Sextet 2	0.49	0.02	49.0	1.40	46.5
	Rel. Area sextets	97%	**Collapsed Feature**	0.65[e]	-0.10[e]	25.8[e]	14.7[e]	3.0
^{56}Fe Hydrothermally treated again goethite + 1mM ^{57}Fe(II)	**Batch #**	3	**Fe(II)**	1.21	2.71		0.51	7.7
	Initial Fe(II)	1.222 mM	**Fe(III) Sextet 1**	0.47	-0.17	48.3	1.06	38.3
	Sorbed Fe(II)	102 µmoles g^{-1}	**Fe(III) Sextet 2**	0.48	0.08	48.9	1.11	23.8
	Rel. Area sextets	62.1%	**Collapsed Feature**	0.65[e]	-0.10[e]	25.8[e]	14.65[e]	30.3

Sample	Experiment		Mössbauer parameters					
			Component	CS[a] ($mm\ s^{-1}$)	QS[b] ($mm\ s^{-1}$)	H[c] (Tesla)	Std(H) or Std(QS)[d] (Tesla) or ($mm\ s^{-1}$)	Area (%)
	Batch #	3	**Fe(II)**	1.25	2.91		0.59	7.5
	Initial Fe(II)	1.078 mM	**Fe(III) Sextet 1**	0.48	-0.16	48.7	1.09	39.6
	Sorbed Fe(II)	81 μmoles g^{-1}	**Fe(III) Sextet 2**	0.49	0.09	49.4	1.26	24.1
	Rel. Area sextets	63.7%	**Collapsed Feature**	0.65 [e]	-0.10 [e]	26.25 [e]	13.75 [e]	28.7
	Oxidized sample		**Fe(III) Sextet 1**	0.49	-0.20	48.6	1.35	45.3
			Fe(III) Sextet 2	0.48	0.04	48.9	1.43	44.4
	Rel. Area sextets	89.7%	**Collapsed Feature**	0.64 [e]	-0.10 [e]	25.8 [e]	14.65 [e]	10.3

[a] Center shift
[b] Quadrupole splitting for doublets and quadrupole shift parameter for sextets
[c] Hyperfine Field
[d] Standards deviation of the Voigt profile for the hyperfine field or quadrupole splitting parameters, respectively
[e] Denotes that the parameter was fixed

Table S2. Fe(II) and Fe total extraction data.

Step	$Fe(II)_{aq}$ (µmol)	Fe(tot) (µmol)	% of sorbed Fe(II) recovered
0.4 M HCl extraction			
Initial $_{aqueous}$	892	891	
Final $_{aqueous}$	591	585	
HCl $_{extracted}$	303	301	100
Sequential extractions			
Initial $_{aqueous}$	1120		
Final $_{aqueous}$	760	750	
Buffer wash $_{extracted}$	80	70	22
$CaCl_2$ $_{extracted}$	60	50	17
NaH_2PO_4 $_{extracted}$	140	140	39

Table S3. Characteristics of goethite after sequential hydrothermal/grinding treatments.

	XRD Cell dimensions			BET
	a **(Å)**	***b*** **(Å)**	***c*** **(Å)**	**(m^2 g^{-1})**
As-synthesized	4.606	9.964	3.027	28
Hydrothermally treated	4.606	9.955	3.023	26
Ground	4.605	9.955	3.022	18
Hydrothermally treated *again*	4.603	9.956	3.022	19

References

1. Amstaetter, K.; Borch, T.; Larese-Casanova, P.; Kappler, A., Redox Transformation of Arsenic by Fe(II)-Activated Goethite (α-FeOOH). *Environmental Science & Technology* **2010,** *44*, (1), 102-108.

2. Pasakarnis, T.; McCormick, M. L.; Parkin, G. F.; Thompson, A.; Scherer, M. M., Fe^{II}aq–Fe^{III}oxide electron transfer and Fe exchange: effect of organic carbon. *Environmental Chemistry* **2015,** *12*, (1), 52-63.

3. Latta, D. E.; Bachman, J. E.; Scherer, M. M., Fe Electron Transfer and Atom Exchange in Goethite: Influence of Al-Substitution and Anion Sorption. *Environmental Science & Technology* **2012,** *46*, (19), 10614-10623.

4. Genin, J. M.; Bauer, P.; Olowe, A. A.; Rezel, D., Mössbauer study of the kinetics of simulated corrosion process of iron in chlorinated aqueous solution around room temperature: The hyperfine structure of ferrous hydroxides and Green Rust I. *Hyperfine Interactions* **1986,** *29*, (1), 1355-1360.

5. Burns, R. G., Intervalence transitions in mixed valence minerals of iron and titanium. *Annual Review of Earth and Planetary Sciences* **1981,** *9*, (1), 345-383.

6. Yoshida, Y.; Langouche, G., *Mössbauer Spectroscopy: Tutorial Book*. Springer Berlin Heidelberg: 2012.

7. Gilbert, B.; Erbs, J. J.; Penn, R. L.; Petkov, V.; Spagnoli, D.; Waychunas, G. A., A disordered nanoparticle model for 6-line ferrihydrite. *American Mineralogist* **2013,** *98*, (8-9), 1465-1476.